Structural and physico-chemical analysis of calcium/ strontium substituted, near-invert phosphate based glasses for biomedical applications

U. Patel,[a] R.M. Moss,[c] K.M.Z Hossain,[a] A.R. Kennedy,[a] E.R. Barney,[a] I. Ahmed,[a] and A.C. Hannon [b]

[a]*Faculty of Engineering, University of Nottingham, Nottingham, NG7 2RD, UK*

[b]*ISIS Facility, Rutherford Appleton Laboratory, Chilton, Didcot, OX11 0QX, UK*

[c]*Department of Medical Physics and Biomedical Engineering, University College London, London, UK*

Revised for Acta Biomaterialia

Keywords: Biomedical glass; Glass structure; Neutron diffraction; Solid state NMR; Phosphate glass; Strontium; Dissolution rate

Abstract

Neutron diffraction, ^{23}Na and ^{31}P NMR and FTIR spectroscopy have been used to investigate the structural effects of substituting CaO with SrO in a $40P_2O_5{\cdot}(16\text{-}x)CaO{\cdot}20Na_2O{\cdot}24MgO{\cdot}x$SrO glass, where *x* is 0, 4, 8, 12 and 16 mol%. The ^{31}P solid-state NMR results showed similar amounts of Q^1 and Q^2 units for all of the multicomponent glasses investigated, showing that the substitution of Sr for Ca has no effect on the phosphate network. The M-O coordinations (M= Mg, Ca, Sr, Na) were determined for binary alkali and alkaline earth metaphosphates using neutron diffraction and broad asymmetric distributions of bond length were observed, with coordination numbers that were smaller and bond lengths that were shorter than in corresponding crystals. The Mg-O coordination number was determined most reliably as 5.0(2). The neutron diffraction results for the multicomponent glasses are consistent with a structural model in which the coordination of Ca, Sr and Na is the same as in the binary metaphosphate glass, whereas there is a definite shift of Mg-O bonds to longer distance. There is also a small but consistent increase in the Mg-O coordination number and the width of the distribution of Mg-O bond lengths, as Sr substitutes for Ca. Functional properties, including glass transition temperatures, thermal processing windows, dissolution rates and ion release profiles were also investigated. Dissolution studies showed a decrease in dissolution rate with initial addition of 4 mol% SrO, but further addition of SrO showed little change. The ion release profiles followed a similar trend to the dissolution rates observed. The limited changes in structure and dissolution rates observed for substitution of Ca with Sr in these fixed 40 mol% P_2O_5 glasses were attributed to their similarities in terms of ionic size and charge.

1. Introduction

Phosphate based glasses containing ions characteristically native to bone (Ca^{2+}, Na^{2+}, Mg^{2+}, PO_4^{3-}) have been widely investigated due to their fully resorbable properties, controlled dissolution rates, and biocompatible nature [1-5]. The ability to control these properties makes phosphate glasses extremely well suited for delivery of therapeutic ions. Their use in both hard and soft tissue repair has been extensively studied [1,6,7] and the benefits of adding these ions into bioactive materials have been summarised by Mouriño *et al*. [8] and Hoppe *et al*. [9].

Research into bioactive glasses has focused on tailoring glass properties to address specific clinical needs. The ability to introduce new oxides to the basic sodium-calcium phosphate glass network is of great interest as it allows properties such as their dissolution rates to be tailored (see for example works studying the effect of MgO [10], TiO_2 [11] and Fe_2O_3 [12]) and the addition of therapeutic ions for controlled release into the body [13].

One of the most common treatments for osteoporosis was administration of low doses (316–634 mg/kg per day Sr^{2+}) of strontium ranelate or strontium chloride for 9-26 weeks. This was shown to reduce bone resorption and stimulate bone formation via increased replication of preosteoblastic cells. This is beneficial since it is the imbalance of bone deposition and resorption which leads to osteoporosis [14-16] and the dual effect of strontium on bone metabolism has been investigated by researchers for use in orthopaedic applications [17-21]. Recent studies have shown that addition of strontium ions to phosphate glasses has the potential to aid treatment of osteoporosis [17-19,22,23]. Strontium is known to follow a similar physiological pathway in humans as calcium, where a large portion accumulates in bone via ionic exchange of calcium for strontium, thus it has been used in bone therapies [24]. However, controversy does exist in the use of strontium in bone health products due to its ability to displace calcium in the bone at high concentrations and reside there, which in turn leads to increased attenuation of x-rays, leading to overestimation of bone mineral density (BMD) values [25,26]. By incorporating strontium into a fully degradable material, it should be possible to achieve a controlled release of strontium into the body over time.

The dissolution rates of phosphate glasses are dominated by their formulation, though factors such as pH and temperature can also have an effect. Multiple factors contribute to this dependence of dissolution on formulation. The two key factors are network connectivity [27] and the arrangement of modifier cations and modifier-chain bonding in the glass. Previous studies have shown that the addition of alkali and alkaline earth oxides to a phosphate network reduced the glass network connectivity by replacing BO (bridging oxygen) with NBO (non-bridging oxygen) in the phosphate backbone [28] and the modifier oxides occupied interstitial spaces between chains of $[PO_4]$ units [29]. The ionic strengths of the modifiers will determine bond strength and this has been shown to influence physical properties such as glass transition temperature and dissolution rates. For example, a highly coordinated modifier cation, with high ionic strength, can increase cross-linking within the glass network, rendering the glass formulation less prone to dissolution [30]. The degradation properties of phosphate glasses are known to be sensitive to the glass structure and understanding the short and medium range order of specific formulations is important to allow glass formulations to be tuned for their potential therapeutic applications.

The dissolution of phosphate-based glasses, explained by Bunker *et al.* [31], occurs via three steps; initially H^+ and OH^- ions are taken up on the surface of the glass via an acid/base reaction until fully saturated. This is followed by a hydration process where ion exchange occurs via an inward diffusion of H^+ molecules and outward diffusion of alkali/alkaline earth cations, releasing chains into solution. The degree of hydration has been shown to be influenced by the concentration of mobile cations on the surface and the ratio of BO to NBO sites in the bulk glass matrix [31-33]. Both of these factors are dependent on the glass composition. This is then followed by hydrolysis of the chains in solution. Dissolution of the glass matrix results in a reduction of alkali ions on the outer surface [31]. External factors such as solution pH and concentration of ions in the solution can also have a strong

effect on dissolution rate, for example a decrease in pH has been shown to accelerate glass dissolution [31].

The aim of this study was to investigate phosphate glass formulations which degraded and released strontium ions at a controlled rate. To achieve this it was desirable to substitute strontium into a previously investigated phosphate host glass formulation, ideally retaining the dissolution rate of this previously optimised glass [4]. To enable this, strontium ions were introduced to the glass network ($40P_2O_5 \cdot (16\text{-}x)\ CaO \cdot 20Na_2O \cdot 24MgO \cdot xSrO$) by substitution for calcium to minimise the changes in the glass structure; cations with the same valence and similar charge to size ratio can be easily substituted within glass structures [34]. The glasses investigated had a fixed P_2O_5 content at 40 mol% which can be considered to be on the verge of an invert phosphate glass formulation. Invert glasses are defined as containing <40 mol% of P_2O_5, where they predominantly consist of pyro- and orthophosphates, thus forming a highly depolymerised network with properties governed by the modifier ions [35,36].

Structural studies examining substitution of calcium for strontium in a bioactive silicate glass formulation ($49.46SiO_2 \cdot 26.38Na_2O \cdot 1.07P_2O_5 \cdot (23.08\text{-}x)CaO \cdot xSrO$; where x= 0, 11.54, 23.08) found a split in the Ca-O, Sr-O, and Na-O nearest neighbour correlations which was attributed to the cations bonding to BO and NBO atoms [23]. This was in agreement with other studies of the sodium environment in silicate glasses [34]. These studies of bioactive silicate glass compositions found that the substitution between two cations within the same periodic group did not disrupt the bonding within the silica glass network.

However, although several studies on the structure of phosphate based glasses have been conducted [37-44], very little is known about the effect of cation substitution on the structure of complex, multicomponent, lower phosphate containing glasses (i.e. for phosphate glasses close to invert glass formulations). This is primarily due to the difficulties associated with the deconvolution of overlapping modifier–oxygen peaks in diffraction data.

In this study, the effect of isostoichiometric substitution of CaO for SrO in a multicomponent phosphate glass fixed with 40 mol% P_2O_5 has been characterised through examination of the structure and properties of the glasses. Neutron diffraction, ^{31}P MAS (magic angle spinning) NMR and ^{23}Na MAS NMR studies have been conducted to understand the short range order and the coordination environment of the modifiers and results have been related to the thermal properties, dissolution rates and ion release profiles of the glasses.

2. Experimental

2.1. Sample preparation

A series of two- (binaries) and five- (multi) component phosphate glasses, with a phosphate to cation ratio of 50:50 and 40:60 respectively, were made using the following precursors; P_2O_5 (Sigma Aldrich, assay 98%), NaH_2PO_4 (Sigma Aldrich, assay ≥99%) , $CaHPO_4$ (Sigma Aldrich, assay 98-105.5%), $MgHPO_4 \cdot 3H_2O$ (Sigma Aldrich, assay ≥97%), and $SrCO_3$ (Sigma Aldrich, assay ≥99%) (See Table 1). Binary compositions with the same P_2O_5 content (40 mol% P_2O_5) as the multicomponent glasses would not form a glass. The weighed precursors were thoroughly mixed and heated in a 5% Au/95% Pt crucible at 350°C for 30 minutes to dehydrate and remove CO_2 before placing the mixture into a

furnace and heated to 1150°C for 1.5h. The melts for the binary samples were quenched between two stainless steel plates and the melts for the multicomponent series were poured into preheated graphite moulds (10°C above the glass transition temperature of each sample). The latter were annealed for 1h, followed by slow cooling to room temperature overnight. The amorphous nature of all the multicomponent glasses was confirmed using a Bruker D500 X-ray diffractometer.

Table 1: Compositions and densities of the samples, with the preparation method indicated by X.

Sample	P_2O_5 (mol%)	CaO (mol%)	Na_2O (mol%)	MgO (mol%)	SrO (mol%)	Melt quenched	Cast rod	Density (g cm^{-3})
CaP_2O_6	50	50	-	-	-	X	-	2.69
$Na_2P_2O_6$	50	-	50	-	-	X	-	2.55
MgP_2O_6	50	-	-	50	-	X	-	2.49
SrP_2O_6	50	-	-	-	50	X	-	3.30
P40	40	16	20	24	-	-	X	2.71
Sr4	40	12	20	24	4	-	X	2.74
Sr8	40	8	20	24	8	-	X	2.79
Sr12	40	4	20	24	12	-	X	2.84
Sr16	40	-	20	24	16	-	X	2.89

2.2. Density, molar volume and free volume

The density of each sample was measured three times using Micromeritics Accupyc1340 pycnometer, with helium as the displacement gas. For each measurement, a series of repeat readings were taken until a series of five results agreed within an error of ± 0.02gcm^{-3}.

2.3. Thermal analysis

DSC measurements (TA Instruments SDT Q600, UK) were collected on 40mg of sample, with a particle size of 45-63 μm. These were heated from 50 °C to 1000 °C at a heating rate of 10 °C/minute under flowing argon gas to determine the glass transition temperature, T_g, crystallisation temperature, T_c, and melting temperature, T_m of each glass sample.

2.4. Spectroscopy

Energy-dispersive X-ray spectroscopy (EDX) was used to determine glass composition. Glass samples were embedded in epoxy resin and ground using SiC paper followed by diamond polishing. Due to the hygroscopic nature of phosphate glass, industrial methylated spirit (IMS, Sigma Aldrich, UK, ≥99.5%) was used as a lubricating medium to prevent degradation of the sample. Samples were then placed in an ultrasonic bath of IMS for 10 minutes and left to dry, followed by carbon coating with a thickness of ~15nm. EDX measurements of composition were carried out using Oxford Instruments INCA EDX system fitted with a Si-Li crystal detector. The EDX system was attached to a Philips XL30 scanning electron and operated in backscattered electron mode, with an accelerating voltage of 20kV and a working distance of 10mm. Analysis was conducted on three separate areas on each sample, and three separate samples were used for each multicomponent composition.

Fourier transform infrared spectroscopy (FTIR) was performed on all multicomponent glasses using a Bruker Tensor-27 Fourier transform infrared spectrometer. Glass samples were ground to a fine

powder (45-63μm) using a mineral mortar and pestle. The samples were scanned in absorbance mode in the region of 4000 to 550 cm^{-1} using a standard attenuated total reflectance (ATR) cell (PIKE Technologies). The spectra were analysed using OPUS™ software, including subtraction of air background.

Solid-state ^{31}P and ^{23}Na MAS NMR spectra were obtained via the EPSRC UK National Solid-state NMR Service at Durham using a Varian VNMRS spectrometer and a 4 mm magic-angle spinning probe with a spin rate of 11-12 kHz. They were recorded using direct excitation at a Larmor frequency of 161.87 MHz for ^{31}P and 105.78 MHz for ^{23}Na NMR. The ^{31}P spectra were obtained with a 300 second pulse delay and 4.4 μs pulse duration and were referenced to 85% H_3PO_4. The ^{23}Na spectra were acquired with a 1 s pulse delay and 1.0 μs pulse duration and were referenced to 0.1 M aqueous NaCl

2.5. Neutron diffraction

Neutron diffraction data were collected on the GEM diffractometer [45] at the ISIS spallation neutron source at Rutherford Appleton Laboratory, UK.

In a neutron diffraction experiment, the differential cross section, $\frac{d\sigma}{d\Omega}$, or total scattering, $I(Q)$ is measured;

$$\frac{d\sigma}{d\Omega} = I(Q) = I^s(Q) + i(Q) \quad (1)$$

where the total scattering from a sample is equal to the sum of the self-scattering, $I^s(Q)$, and the distinct scattering, $i(Q)$. Coarsely ground binary samples were contained in vanadium cylinders with a diameter of 10.3 mm and wall thickness of 40 μm. The Sr-series glasses were cast into rods and fixed to sample holders, eliminating the need for a container. In addition to collecting interference patterns for each sample, data for the empty cans, a vanadium rod and the empty instrument were also obtained in order to carry out the appropriate corrections (for attenuation, multiple scattering and self-scattering) using the programme GUDRUN [46] and ATLAS [47] software.

The total correlation function ($T(r)$) can then be calculated via Fourier transformation of $i(Q)$.

$$T(r) = T^0(r) + \frac{2}{\pi}\int_0^\infty Qi(Q)M(Q)\sin(rQ)\,dQ \quad (2)$$

Where $T^0(r)$ is the average density contribution to the correlation function ($T^0(r) = 4\pi r\rho_0\left(\sum_{l=1}^{N} c_l\bar{b}_l\right)^2$), r is the distance between atoms, ρ^0 is the average atomic number density, N is the number of elements in the sample, and c_l and $\bar{b}_l$ are respectively the atomic fraction and coherent scattering for element l. $M(Q)$ is a modification function (e.g. the Lorch [48] function or a step function), which is used to take account of the fact that experimental data are only available up to some finite maximum momentum transfer, $Q_{\max}$, not infinity as in Equation (2).

Structural information was obtained by fitting $T(r)$, which is the weighted sum of all the possible partial correlation functions, $t_{ll'}(r)$, given by

$$T(r) = \sum_{ll'} c_l\,\bar{b}_l\,\bar{b}_{l'}\,t_{ll'}(r) \quad (3)$$

At short distances, where a peak in $T(r)$ arises from only one particular pair of elements (l and l'), the peak area, $A_{ll'}$, interatomic distance, $r_{ll'}$, and the coordination number, $n_{ll'}$, can be calculated, according to:

$$n_{ll'} = \frac{A_{ll'} \; r_{ll'}}{(2-\delta_{ll'})c_l \bar{b}_l \bar{b}_{l'}} \tag{4}$$

where $\delta_{ll'}$ is the Kronecker delta.

2.6. Dissolution and ion release studies

The dissolution studies were conducted using glass discs (c.a. 9mm Ø by 5mm width) degraded in 30ml of ultra-pure water (18.2 MΩ) at 37ºC. The medium was replenished at each time point (1, 3, 7, 14, 21 and 28 days), and replaced with 30ml of fresh ultra-pure water. Conducting pH measurements were performed on the water that was removed at each time point. This study was repeated using discs with a dimension of c.a. 9mm Ø by 10mm width in deionised water (DI) and phosphate-buffered saline (PBS). The release of Ca^{2+}, Na^{+}, Mg^{2+} and Sr^{2+} from the dissolution media at each time point were quantified using an ICS-1000 ion chromatography system (Thermo Scientific, Dionex, UK). An eluent of 20mM methanosulfonic acid (Sigma-Aldrich) was used. All specimens were analysed using a Dionex IonPac® CS12A 2mm x 250mm analytical column, and analysed under suppressed conductivity (CSRS 300 2mm, Thermo Scientific, Dionex). Results were calculated against a four-point calibration curve using a Combined Six Cation Standard II and Strontium (Sr^{2+}) 1000mg/l in water (Thermo Fisher Scientific). A stock solution containing the cations was prepared. From which serially diluted cation standards were prepared at the following dilution factors; 1:1024, 1:256, 1:64 and 1:16. Data analysis was performed using Chromeleon® software, and the cumulative release per unit area of each sample was calculated.

2.7. Statistical analysis

For the dissolution measurements, the average values and standard deviation were calculated for a sample size *n*=3. Statistical analysis was performed using GraphPad Prism 7.01 (GraphPad Inc., San Diego, CA). One-way analysis of variance (ANOVA) was calculated followed by Tukey's multiple comparison test. The mean difference was considered to be significant at 0.05 and 95% confidence interval.

The errors on the data points in the measured neutron spectra were determined by counting statistics (*i.e.* for *N* counts the standard deviation is $\sqrt{N}$), and these were propagated through the various stages of data reduction and correction so as to determine the standard deviation on the data points for $i(Q)$. The statistical errors on $i(Q)$ were then propagated through to the Fourier transform, $T(r)$, according to the theory presented by Toby and Egami [49]. The statistical errors on $T(r)$ were taken into account in the fits to $T(r)$, giving rise to the statistical errors on the fit parameters reported in Tables 5, 6 and 7. No attempt to take account of systematic errors was made.

3. Results

The bulk characterisation results presented here are those of the multicomponent glasses in the series P40, Sr4, Sr8, Sr12 and Sr16. The binary glasses were fabricated and analysed in order to aid deconvolution of the neutron diffraction correlation functions measured for the multicomponent glasses.

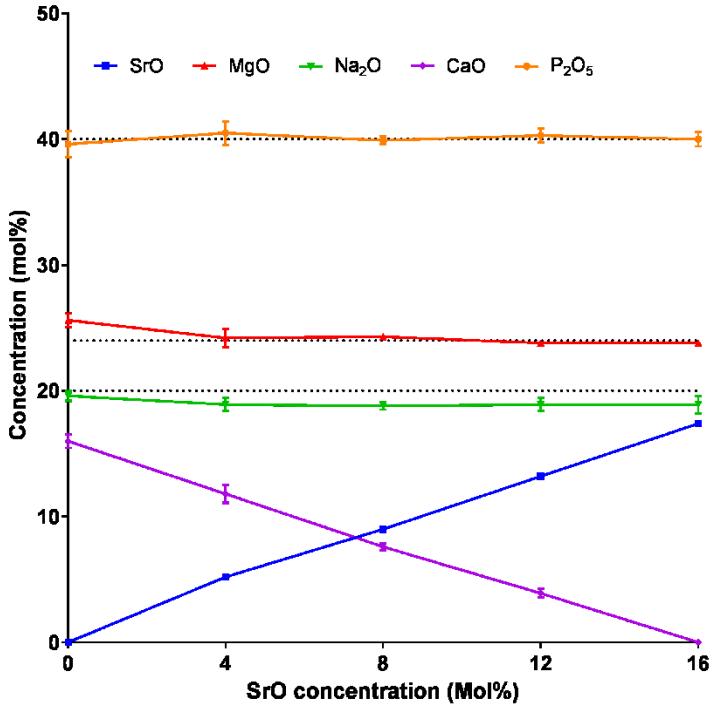

Fig. 1 Composition of multicomponent glass samples as measured by EDX. Dotted lines represent the target value.

3.1. Glass characterisation

Fig. 1 shows the results of the EDX measurements on the multicomponent glasses. All compositions were confirmed to be within the 1-2% of the target composition, and hence the nominal compositions were used for the analysis of the structural studies. A ~1 mol % reduction in CaO was accompanied by a SrO increase of ~1 mol% compared to that of the target values. The density and molar volume for the multicomponent glasses are shown in Fig. 2. The density increases by ~7% from 2.71 to 2.89 g/cm^3 as SrO is substituted for CaO, whilst the molar volume increases by ~2% (from 32.41 cm^3 mol^{-1} to 33.02 cm^3 mol^{-1}).

Fig. 3 and Table 2 show the results of the DSC measurements on the multicomponent glasses. A distinctive crystallisation peak is observed, and initially its temperature, T_c, increases from 591°C for the host glass composition (P40) to 609°C with the addition of 4 mol% of SrO (Sr4), followed by a single melting peak. However, as more strontium is added to the glass (Sr8 – Sr16) the crystallisation temperature steadily decreases to 565°C and the melting peak becomes broader, less defined and reduced in area. With increasing addition of strontium to ≥ 8mol% SrO, two melting features were observed, which shifted to lower temperatures. This behaviour, and the broadening of the crystallisation peak, are attributed to the presence of more than one crystalline phase. There is a

small overall decrease of only 7 °C in T_g as strontium substitutes for calcium, and a much more marked decrease in the melting temperature, T_m.

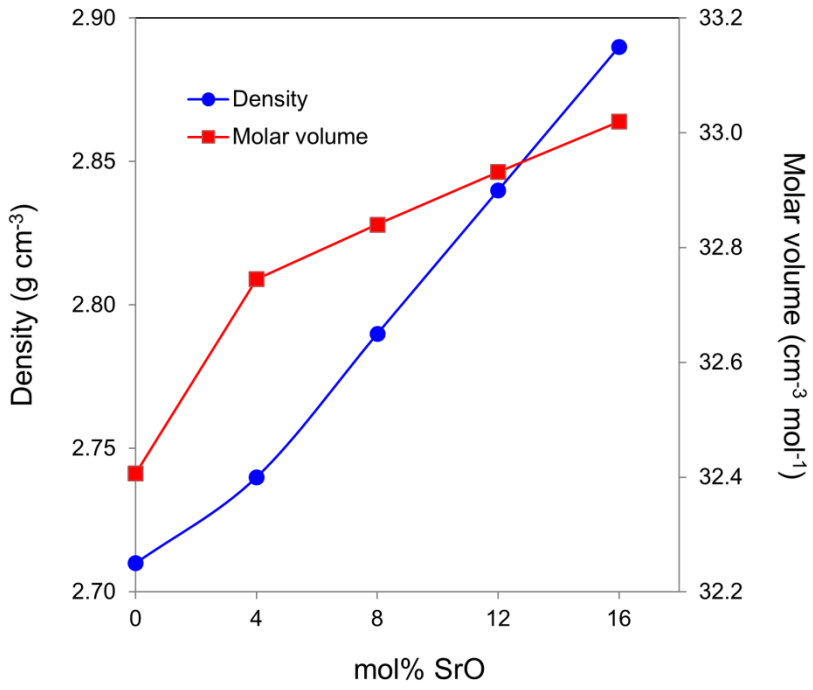

Fig. 2 Density and molar volume of the multicomponent $40P_2O_5{\cdot}(16\text{-}x)CaO{\cdot}20Na_2O{\cdot}24MgO{\cdot}xSrO$ glasses.

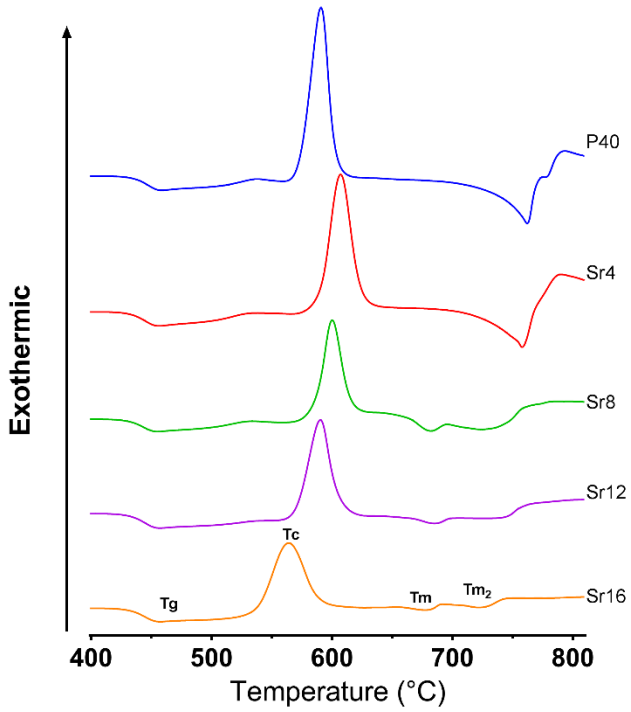

Fig. 3 DSC traces of the multicomponent glass samples, showing T_g, T_c and T_m.

Table 2: Glass transition, T_g, crystallisation, T_c, onset of crystallisation, T_{onset}, and melting temperatures, T_m, for each composition is given, together with the calculated thermal processing window, T_{onset}-T_g, of each glass.

Glass code	T_g (°C)	T_{onset} (°C)	T_c (°C)	T_m (°C)	T_{m2} (°C)	T_{onset}-T_g (°C)
P40	450	573	591	762		123
Sr4	447	588	609	759		141
Sr8	447	582	601	734	854	135
Sr12	447	571	589	685	742	124
Sr16	443	538	565	679	725	95

Typical errors on the temperature values are ±1 °C or less.

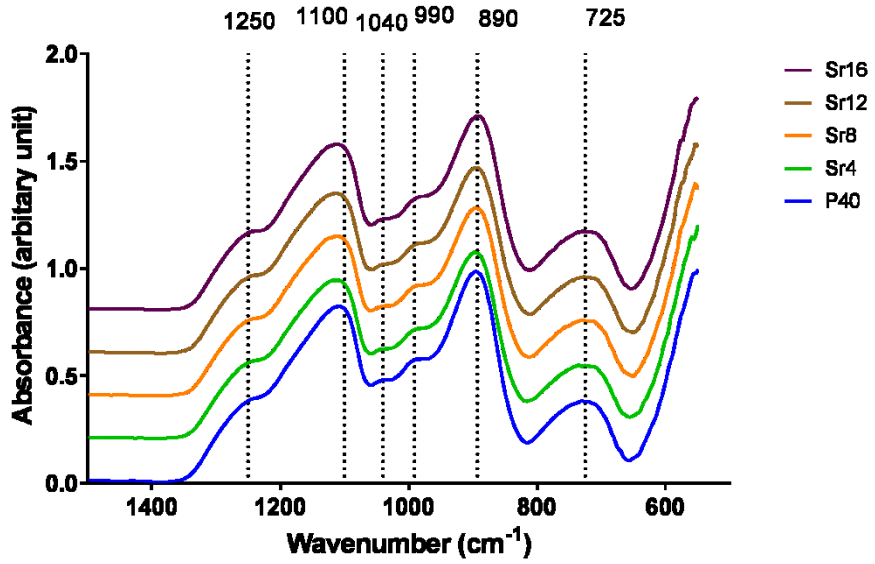

Fig. 4 FTIR spectra for the multicomponent glasses. The dotted lines indicate prominent bands in the spectra, and their positions are given in cm^{-1}.

3.2. Spectroscopy

Fig. 4 shows the FTIR spectra for the multicomponent glasses. The prominent band positions (in cm^{-1}) are indicated by dotted lines.

Fig. 5 shows the solid-state ^{31}P and ^{23}Na MAS NMR spectra for the multicomponent glasses. The two dominant isotropic peaks in the ^{31}P NMR spectra (Fig. 5a) are at *ca.* -8.0 ppm and -22 ppm. Fig. 5b shows the ^{23}Na NMR spectra, which exhibit a single, broad, slightly asymmetric peak at approximately 15 ppm [50,51].

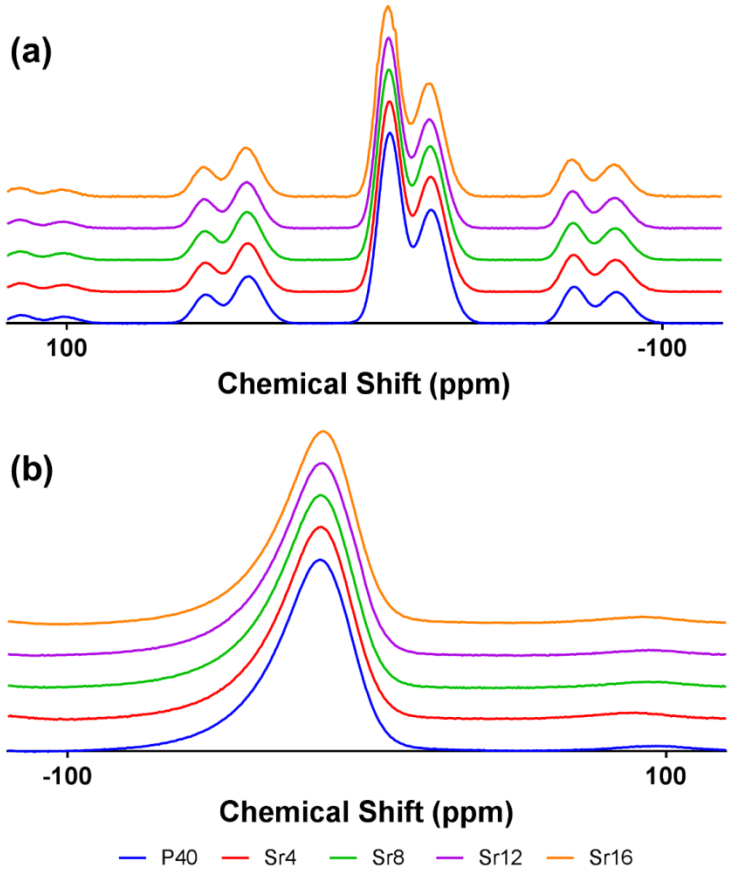

Fig. 5 Solid state MAS NMR spectra of the multicomponent glasses: (a) ^{31}P, and (b) ^{23}Na.

3.3. Neutron diffraction

The neutron diffraction measurements of the distinct scattering function, $i(Q)$, for the binary metaphosphate glasses are shown in Fig. 6a, with the main graph showing the low Q region in order to display the most prominent changes, and the insert showing the data to a maximum Q of 50 Å^{-1}, as used to Fourier transform the data. This high value of Q_{max} yields a narrow resolution in real-space. The high penetration of neutrons and high resolution in reciprocal-space gives good sensitivity to the presence of crystallinity, and hence the amorphous nature of each sample was confirmed via the lack of Bragg peaks. Neutron diffraction is highly sensitive to the presence of hydrogen in a sample, due to the high incoherent scattering cross-section of hydrogen, and thus the presence of water contamination is readily detected; there was no evidence for water contamination of the samples. The neutron diffraction data presented here are available from the ISIS Disordered Materials Database [52]. The first sharp diffraction peak (FSDP) is at 1.56 Å^{-1} for MgP_2O_6, and shifts slightly to higher Q with increasing alkaline earth radius (see Fig. 6a). In contrast, the diffraction patterns for the multicomponent glasses show almost no change in the FSDP with composition (see Fig. 6b).

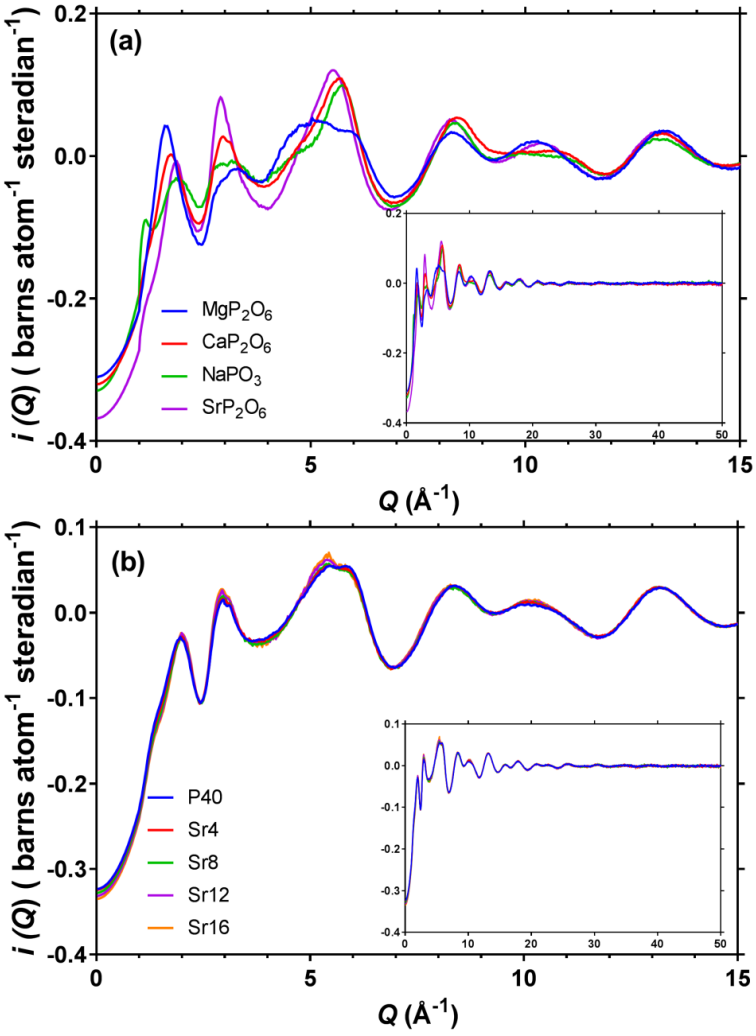

Fig. 6 Distinct scattering, $i(Q)$, of (a) binary metaphosphate, and (b) multicomponent glasses $40P_2O_5{\cdot}(16\text{-}x)CaO{\cdot}20Na_2O{\cdot}24MgO{\cdot}xSrO$ glass, where x is 0, 4, 8, 12 and 16 mol% SrO.

Fig. 7a shows the total correlation functions, $T(r)$, for the binary metaphosphate glasses, and Fig. 7b displays the corresponding $T(r)$ for the multicomponent glasses. The step modification function was used to calculate $T(r)$ (see equation 2) for the region at low r preceding the dotted line (at 1.8 Å), and the Lorch modification function [48] was used for the region subsequent to the dotted line at high r. The step modification function results in narrower real-space resolution, at the expense of much larger termination ripples either side of real peaks, and the use of the step function at low r reveals a splitting of the P-NBO and P-BO peaks at *ca.* 1.5 Å and *ca.* 1.6 Å respectively (Fig. 7a and 7b).

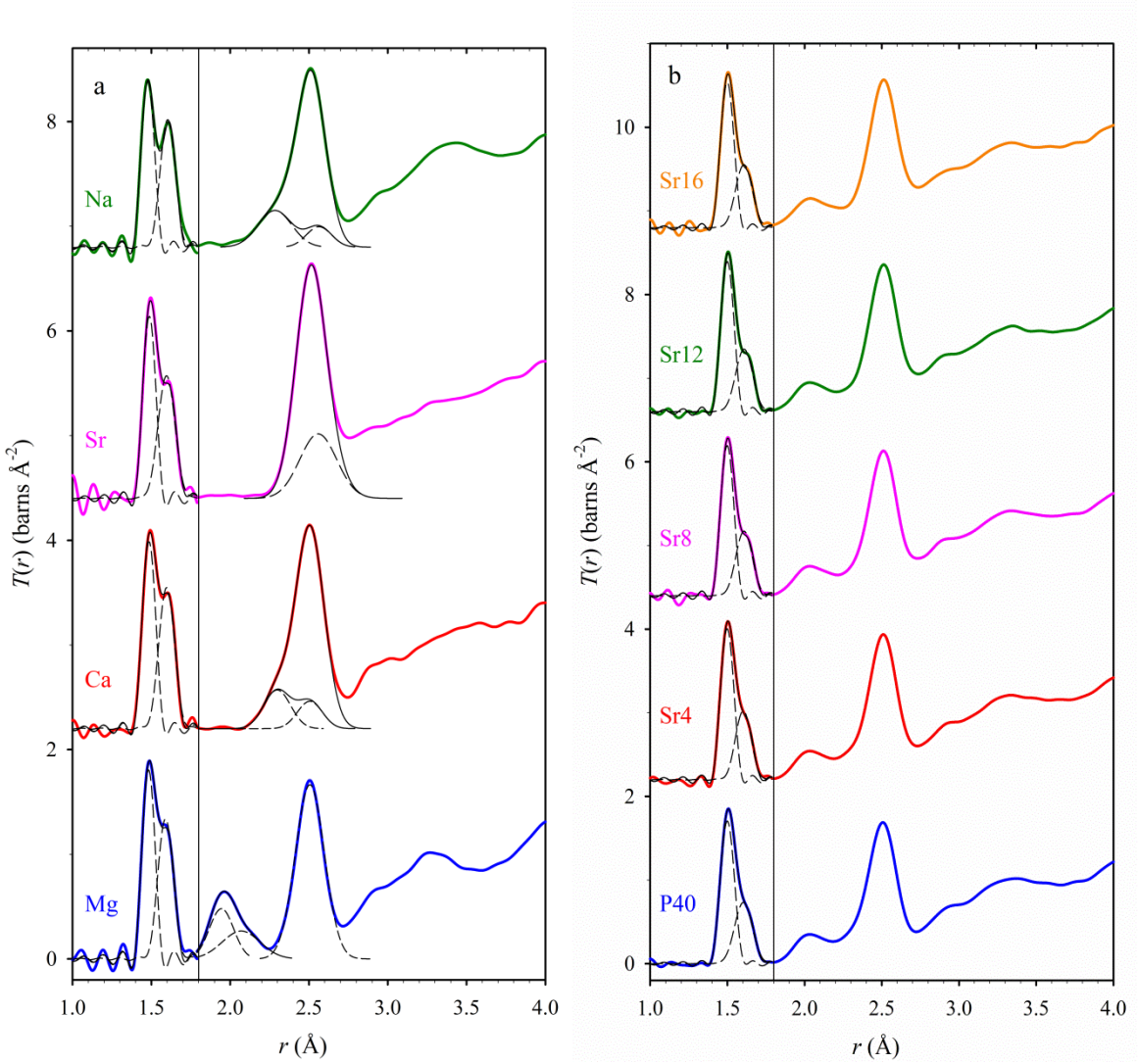

Fig. 7 Total correlation functions, $T(r)$, of (a) binary glasses, and (b) multicomponent glasses, where the region before the vertical line at 1.8 Å was Fourier transformed using the step modification function, and the region after the dotted line was Fourier transformed using the Lorch modification function [48]. Thick coloured lines are for experimental data, whilst thin black lines indicate fitted peaks (individual components are shown dashed, and sums of components are shown continuous).

3.4. Dissolution and ion release

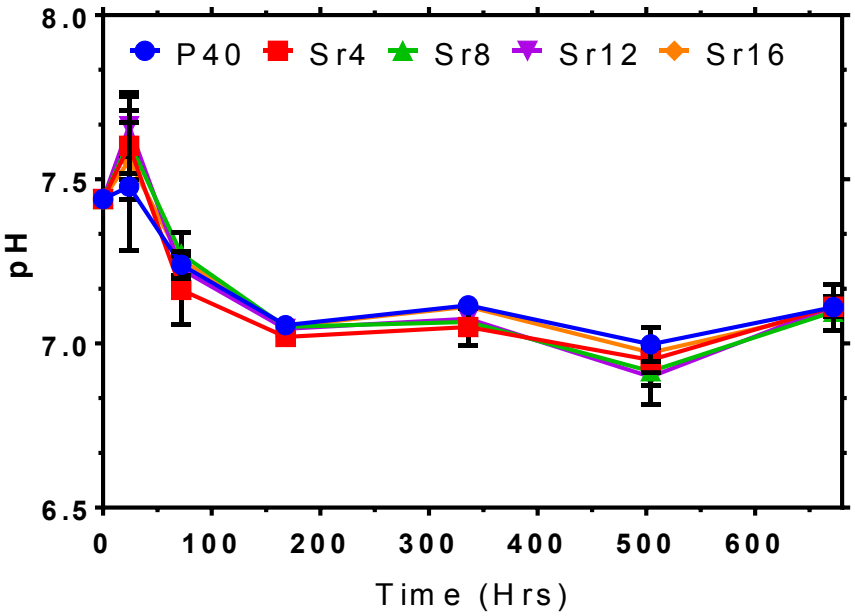

Fig. 8 The pH of the dissolution media (ultra-pure water) at each time point for each of the multicomponent glasses.

The pH of the water during the dissolution studies is shown in Fig. 8, whilst Fig. 9 shows the average mass loss per unit area for multicomponent glasses in ultra-pure water, as measured by the procedure described in Section 2.6. The inset to Fig. 9 shows the dissolution rates for the multicomponent glasses determined via the slope of best fit for each composition in all three media tested. The initial addition of SrO to the glass (adding 4 mol% SrO) caused a reduction in the dissolution rate.

The ion release studies were conducted for the following cations, Ca^{2+}, Na^{+}, Mg^{2+} and Sr^{2+}, as shown in Fig.10. The profiles show that Na^{+} and Mg^{2+} follow a similar trend to the dissolution study where P40 released the highest concentration of cations over time, and strontium-containing glasses showed a consistent release of cations ranging from 0.27ppm for Sr4 at 24 hours to 50.95ppm for Sr16 at 672 hours.

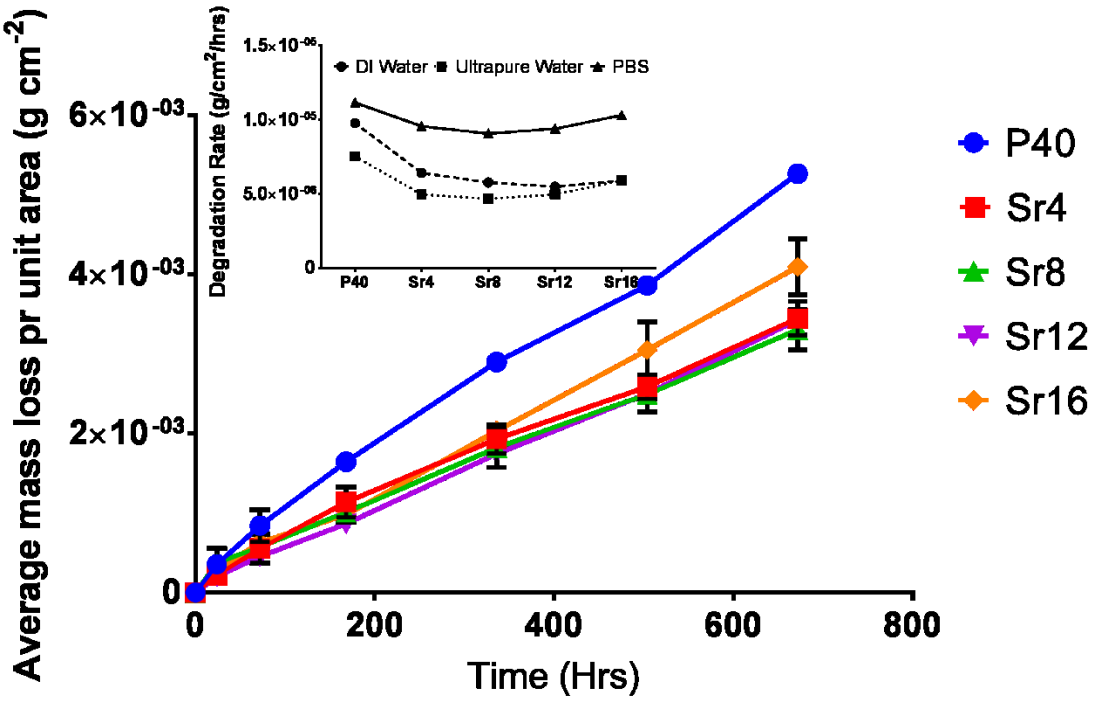

Fig. 9 The average mass loss per unit area (g cm^{-2}) for multicomponent glasses in ultra-pure water. The insert shows the dissolution rate (g/cm^2/hrs) for each multicomponent glass (*n*=3) in ultra-pure water, deionised water (DI) and phosphate buffered saline (PBS) – see text for details.

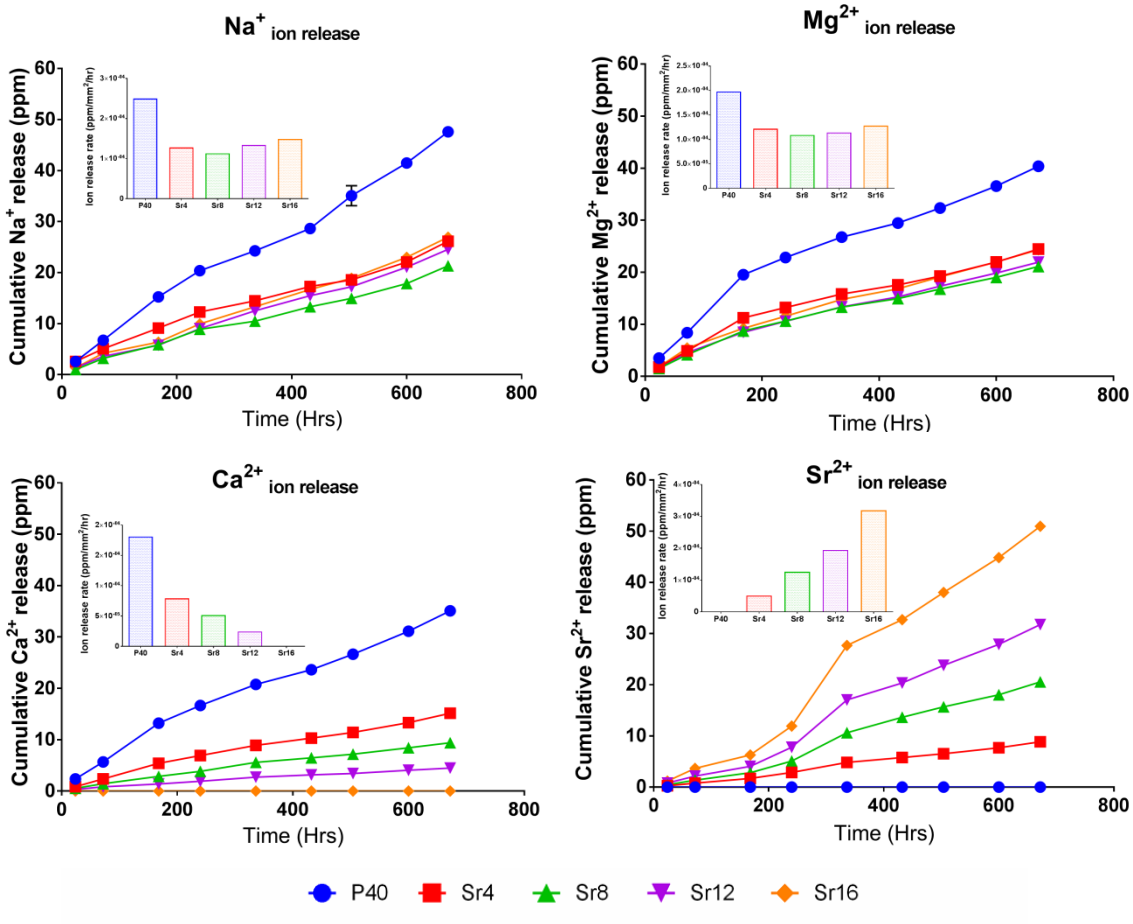

Fig. 10 Cumulative cation release profiles from the multicomponent glasses investigated, which were degraded in ultra-pure water. The inset on each graph shows the ion release rates normalised to the surface area.

4. Discussion

4.1. Glass characterisation

Similar increases/decreases in compositions and error margins to those shown in Fig. 1 have also been reported previously for phosphate glasses and such discrepancies were attributed to losses occurring during melting, and/or due to the initial compositions of the precursor salts themselves, in particular those containing phosphate, due to its hygroscopic nature [4,53-55]. The atomic mass of Sr is more than double that of Ca, and it is by far the heaviest element in the samples; this leads to the relatively large 7% increase in mass density as SrO is substituted for CaO (see Fig. 2 and Table 3). Also, the ionic radius (and hence the ionic volume) of Sr^{2+} is larger than that of Ca^{2+} [56], and this leads to the smaller 2% increase in molar volume as SrO is substituted for CaO. The changes observed with increasing SrO content are consistent with the results of a previous study [19] which reported a 0.04 g/cm^3 increase on substituting 5mol% SrO for Na_2O in a series of $50P_2O_5{\cdot}(20\text{-}x)Na_2O{\cdot}30CaO{\cdot}x$SrO glasses (with x = 1, 3 and 5 mol% SrO). Al Qaysi *et al*. [55] also reported a linear

change in density from 2.6 g/cm^3 to 3.0 g/cm^3 when substituting SrO for CaO in $50P_2O_5{\cdot}10Na_2O{\cdot}5TiO_2{\cdot}(35\text{-}x)CaO{\cdot}x$SrO glasses (with x = 0, 3.5, 17.5 and 35 mol% SrO).

Table 3: Simple properties of calcium and strontium ions, relating to density and molar volume.

Ion	Atomic mass (amu)	Ionic radius [56] (Å)	Ionic volume (Å^3)
Ca^{2+}	40.08	1.00	4.19
Sr^{2+}	87.62	1.18	6.88

Our DSC results show that, when Sr substitutes for Ca, the general overall trend is for a small decrease in T_g, and a larger decrease in T_m (see Table 2). The reason for this behaviour is that (as is discussed below in relation to the neutron diffraction results) Sr-O bonds are weaker than Ca-O bonds [19], and this effect is more significant than any change in the degree of cross-linking of the network. Lakhkar *et al*. [57] have observed similar results to those reported here when substituting SrO for CaO in $50P_2O_5{\cdot}(30\text{-}x)CaO{\cdot}17Na_2O{\cdot}3TiO_2{\cdot}x$SrO glasses (where x = 0, 1, 3, 5 mol% SrO). Furthermore, Abou Neel *et al*. [19] showed that when Sr^{2+} substituted for Na^+, a monovalent cation, in $50P_2O_5{\cdot}(20\text{-}x)\ Na_2O{\cdot}30CaO{\cdot}x$SrO glasses (where x = 0, 1, 3 and 5 mol% SrO), a large increase in T_g, from 383 to 428 °C was observed. Since Sr is divalent, Sr-O bonds are significantly stronger than Na-O bonds.

Studies of silicate glass systems [18,22] have shown that, in contrast to the behaviour of T_g for phosphate glasses, the substitution of strontium for calcium results in an increase in T_g, and it has been suggested that this is due to the expansion and disruption of the silicate glass network with increased strontium due to the larger ionic radius of Sr compared to Ca. It may be that the different behaviours for silicates and phosphate arise due to the lower connectivity of the phosphate network, which is a consequence of the larger number of NBOs in phosphates.

The DSC traces of our multicomponent glasses show two melting features for ≥ 8mol% SrO, and also the crystallisation peak is broader for higher SrO content (see Fig. 3 and Table 2). A recent study [55] investigating the substitution of CaO for SrO in glasses with a fixed P_2O_5 content of 50mol% found that increasing the SrO content led to a more prominent melting peak (which was not apparent in this study), and a reduction in the thermal processing window. The presence of two T_m peaks for glasses with fixed P_2O_5 contents of 45 and 50 mol% has previously been correlated with the following two dominating crystal phases; sodium calcium phosphate ($NaCa(PO_3)_3$), and a beta calcium metaphosphate (CaP_2O_6), as reported by Ahmed *et al*. [1] when investigating ternary $50P_2O_5{\cdot}40CaO{\cdot}10Na_2O$ and $55P_2O_5{\cdot}35CaO{\cdot}10Na_2O$ glass systems. They reported that the predominant crystal phase in both 45 and 50 mol% P_2O_5 ternary glasses was sodium-calcium phosphate. A $NaCa(PO_3)_3$ crystal phase was also found to be dominant in a previous study by Lakhkar *et al*. [58] when investigating CaO substitution with SrO in $0.5P_2O_5{\cdot}0.15Na_2O{\cdot}0.05TiO_2{\cdot}(0.3\text{-}x)CaO{\cdot}x$SrO glasses.

The materials thermal processing window; i.e. the gap between T_g and the onset of crystallisation, T_{onset}, can provide a good indication of the thermal stability of a glass system [59]. The thermal processing window data in Table 2 shows that addition of a fifth component to the glass system (i.e. 4 mol% of SrO) increased the thermal processing window from 123°C to 141°C. This could be explained by the effect of increasing the crystallisation barrier, thus increasing the energy barrier for

the rearrangement of atoms in order to form a critical size defect i.e. the entropy of mixing increases [36,53]. Further substitution of CaO with SrO resulted in a gradual decrease in the thermal processing window which is suggested to be due to the lower field strength of Sr^{2+} (0.28 valence/Å^2) compared to Ca^{2+} (0.33 valence/Å^2) according to Dietzel [60,61]. This, correlated with the observation that the calcium free (Sr16) glass composition had to be cooled much more rapidly than the others to form a glass, agrees well with the work of Lee *et al*. [61,62] who observed that a higher tendency of crystallisation occurred with increasing SrO content in a $30P_2O_5{\cdot}7MgO{\cdot}3TiO_2{\cdot}(60\text{-}x)CaO{\cdot}xSrO$ and $30P_2O_5{\cdot}7Na_2O{\cdot}3TiO_2{\cdot}(60\text{-}x)CaO{\cdot}xSrO$ (mol %) glass system where *x* is 0-60. The narrowing of the thermal processing window with increasing SrO, may potentially make thermal post processing (such as extrusion and fibre drawing) of high strontium content phosphate glasses more difficult than for lower strontium containing formulations.

4.2. Fourier transform infrared spectroscopy

The assignments of the bands in the FTIR spectra (Fig. 4) are as follows: The first two prominent absorption bands at 725 and 890 cm^{-1} are due to symmetric and asymmetric stretching of P-O-P linkages respectively [63]. The bands near 990 and 1100 cm^{-1} have been assigned respectively to symmetric and asymmetric stretching of chain end units associated with Q^1 units [63,64], whilst the 1250 cm^{-1} band has been assigned to the asymmetric stretch of a Q^2 chain unit [55,64-66] (where the *n* in Q^n refers to the number of BO atoms in the tetrahedral PO_4 unit). A small feature at 1040 cm^{-1} is assigned to the symmetric stretch of NBOs in Q^1 groups [65-67]. Both the peak intensities and positions remained constant for all multicomponent glasses studied, suggesting similarities in the structure of the phosphate part of the network between all compositions. Al Qaysi *et al*. [55] investigated the FTIR spectra of Sr-containing phosphate glasses in the composition $50P_2O_5{\cdot}10Na_2O{\cdot}5TiO_2{\cdot}(35\text{-}x)CaO{\cdot}xSrO$ (where *x*=0, 3.5, 17.5 and 35), which showed an unexpected decrease in intensity for peaks at 900cm^{-1} associated with P-O-P asymmetric stretching of Q^2 units and an increase in peak intensity at 1100cm^{-1} associated with Q^1 units with increasing Sr content. The lack in variation between the samples examined in this study using FTIR was attributed to the fact that the O/P ratio (3.25) was constant for each sample, thus not influencing the phosphate network structure.

4.3. Nuclear magnetic resonance spectroscopy

The two dominant isotropic peaks in the ^{31}P NMR spectra at *ca.* -8.0 ppm and -22 ppm (Fig. 5) are ascribed to Q^1 and Q^2 units respectively [28,63]. The relative intensity of these features remained constant with Ca/Sr content, supporting the analysis of the FTIR spectra. This behaviour arises due to the oxygen concentration in the glasses which does not change. For an alkali or alkaline earth phosphate glass with a composition of 100*y* mol% P_2O_5, with *y* in the range from 0.5 to 0.333, there are expected to be only Q^2 and Q^1 units, with an abundance $Q^1=(1\text{-}2y)/y$ (and $Q^2=1\text{-}Q^1$). For the multicomponent glasses, *y*=0.4, and hence equal numbers of Q^2 and Q^1 units are expected. The fact that equal numbers are observed (Table 4) is evidence that all of the modifiers in the glass are indeed acting as network modifiers, and not as network formers. If the phosphate glass contains only Q^2 and Q^1 units, then the average number of BO atoms in a PO_4 unit is given by

$$N_{\mathrm{BO}} = 2 - Q^1 \qquad (5)$$

This is also sometimes referred to as network connectivity [27]. Here, Q^n indicates the fraction of P with *n* bonds to bridging oxygen (BO), as determined by ^{31}P NMR.

This study showed a constant network connectivity $N_{\mathrm{BO}} \approx 1.5$ as given in Table 4. This corresponds to the fact that the overall modifier content was constant throughout the glass series. In summary, the ^{31}P MAS NMR and FTIR results show no evidence for changes in the phosphate part of the network as Sr substitutes for Ca, and this outcome is predicted to have negligible effects on the dissolution rate of these glasses. If the phosphate glass contains only Q^1 and Q^2 units, and there are no rings in the structure, then the average number of PO_4 tetrahedra in a chain is $\overline{N} = 2/Q^1$. Thus the average length of chains in our multicomponent glasses is four tetrahedra. This result is based on the assumption that two Q^1 units are required to terminate the ends of a chain, with Q^2 units between the ends. However, it is also assumed that there are no rings of PO_4 units. For compositions close to metaphosphate (O/P = 3) it has been shown that cyclic phosphate ring structures can also exist [68], necessitating the formation of shorter chains or phosphate dimers (i.e. pyrophosphates).

The ^{23}Na NMR spectra (Fig. 5b) exhibit a single, broad, slightly asymmetric peak at approximately 15 ppm [50,51]. Detailed information on the chemical environment for sodium is difficult to obtain due to both the broadening that arises from the distribution of bond angles and the inability to eliminate second-order quadrupolar interactions [50,51]. A study of the sodium environment in a binary sodium tellurite glass system found that increasing concentration of Na_2O in the glass, caused a change in chemical shift in the ^{23}Na NMR spectra, which was attributed to a decrease in the sodium-oxygen coordination from six to five [69]. The lack of change in chemical shift in this study indicated that substituting CaO for SrO had no effect on the local environment of sodium atoms in the glass.

Table 4: Chemical shifts (ppm referenced using H_3PO_4) and relative concentrations of Q^n units determined by solid-state ^{31}P MAS NMR of each composition investigated and the numbers of bridging oxygens (BOs) and non-bridging oxygens (NBOs) per PO_4 unit, calculated using equation 5.

Glass code	Relative intensity at -8 ppm /% (Q^1)	Relative intensity at -22 ppm /% (Q^2)	N_{BO}	N_{NBO}
P40	49	51	1.51	2.49
Sr4	49	51	1.51	2.49
Sr8	49	51	1.51	2.49
Sr12	50	50	1.50	2.50
Sr16	49	51	1.51	2.49

4.4. Neutron diffraction

Due to the complexity of the multicomponent glasses, extracting coordination information for each of the cations in the glass would be extremely difficult; each of the peaks in the correlation function arising from modifier-oxygen bonds overlaps with at least one other. In the case of the Sr-O peak, of primary interest for this study, there is overlap with peaks arising for Ca-O and Na-O bonds and O...O distances. To provide additional information with which to guide the fits to the correlation functions for the multicomponent glasses, neutron diffraction patterns were measured for relevant binary

metaphosphate glasses (CaP_2O_6, SrP_2O_6, MgP_2O_6 and $NaPO_3$) in addition to the multicomponent glasses. Modifier-oxygen peak positions, widths and areas from fitting the correlation functions for the binary metaphosphate glasses were used to aid in the interpretation of the neutron diffraction data from the multicomponent glasses.

4.4.1 Diffraction patterns

For the binary metaphosphate glasses the FSDP shifts slightly to higher *Q* with increasing alkaline earth radius (Fig. 6a). This shift is surprising, because the position of the FSDP arises from the typical size of the cages formed by the network [70]. It has previously been suggested, on the basis of molar volume studies, that an expansion of the silicate network occurs when strontium is substituted for calcium in silicate glasses [17]. However, the FSDP shift does not provide support for an expansion of the phosphate network as Sr substitutes for Ca. In contrast, the diffraction patterns for the multicomponent glasses show almost no change in the FSDP with composition (see Fig. 6b), suggesting that the size of the network cages does not change significantly as Sr substitutes for Ca.

4.4.2 The P-O coordination

The total correlation functions, $T(r)$, exhibit P-NBO and P-BO peaks at *ca.* 1.5 Å and *ca.* 1.6 Å respectively (Fig. 7a and 7b). Table 5 gives the parameters obtained by fitting these two peaks using the PFIT correlation function fitting software [71,72], which takes into account the real-space resolution function appropriate to the choice of modification function. For these fits, the correlation function obtained using the step modification function was fitted. In order to obtain reliable results, consistent between the samples, it was necessary to constrain the ratio of the two coordination numbers for P-NBO and P-BO. For an alkali or alkaline earth phosphate glass with a composition of 100*y* mol% P_2O_5, the ratio is $n_{\text{P-BO}}/n_{\text{P-NBO}}=4y-1$, and hence it was constrained to be 1.0 for the binary metaphosphate glasses, and to be 0.6 for the multicomponent glasses (consistent with the ^{31}P NMR results for these samples given in Table 4). The bond lengths and peak widths obtained are consistent with previous high real-space resolution studies [39], and in particular similar increases in both bond lengths with modifier content have been found previously. Total P-O coordination numbers from 3.77 to 4.00 were found; the expected P-O coordination number of these tetrahedral glasses is four, but it is common for the experimental values to be slightly lower than the expected value due to the damping of peaks at high *r* arising from *Q*-resolution (in reciprocal-space) [72,73]. It can also be noted that there is less variation in bond lengths amongst the multicomponent glasses than is observed for the binary glasses, indicating that the substitution of calcium for strontium has very little effect on the P-O bond lengths.

Table 5: The phosphorus coordination in the binary and multicomponent glasses, from fitting $T(r)$ obtained using a step modification function.

Sample	**Atom pair $l - l'$**	**Bond length ($r_{ll'}$/Å)**	**Bond length variation ($\langle u_{ll'}^2 \rangle^{1/2}$/Å)**	**Coordination number ($n_{ll'}$)**
MgP_2O_6	P-NBO P-BO **P-O sum**	1.4822 (4) 1.5998 (7)	0.0347 (5) 0.0465 (6)	1.92 (1) 1.92 (1) **3.83 (2)**
CaP_2O_6	P-NBO P-BO **P-O sum**	1.4848 (4) 1.5969 (6)	0.0375 (4) 0.0483 (5)	2.00 (1) 2.00 (1) **4.00 (2)**
SrP_2O_6	P-NBO P-BO **P-O sum**	1.4869 (4) 1.5962 (8)	0.0356 (4) 0.0527 (7)	1.88 (1) 1.88 (1) **3.77 (2)**
$Na_2P_2O_6$	P-NBO P-BO **P-O sum**	1.4776 (8) 1.604 (1)	0.0365 (8) 0.046 (1)	1.93 (2) 1.93 (2) **3.86 (4)**
P40	P-NBO P-BO **P-O sum**	1.49995 (5) 1.6039 (1)	0.04196 (5) 0.0565 (1)	2.458 (2) 1.475 (1) **3.932 (3)**
Sr4	P-NBO P-BO **P-O sum**	1.4988 (2) 1.6031 (6)	0.0386 (3) 0.0494 (6)	2.435 (9) 1.461 (5) **3.90 (1)**
Sr8	P-NBO P-BO **P-O sum**	1.4990 (1) 1.6079 (3)	0.0383 (1) 0.0522 (3)	2.407 (5) 1.444 (3) **3.851 (8)**
Sr12	P-NBO P-BO **P-O sum**	1.4997 (2) 1.6083 (7)	0.0383 (3) 0.0541 (6)	2.41 (1) 1.445 (7) **3.85 (2)**
Sr16	P-NBO P-BO **P-O sum**	1.4992 (3) 1.6070 (8)	0.0394 (3) 0.0530 (7)	2.38 (1) 1.430 (6) **3.81 (2)**

4.4.3 Modifier coordination in binary metaphosphates

The region of $T(r)$ from *ca.* 1.8 Å to *ca.* 2.7 Å has contributions from modifier M-O bonds, and also from O…O distances in PO_4 tetrahedra at *ca.* 2.5 Å. Whereas the P-O bonds can be resolved into two separate types of bond with distinctively different lengths, differing by ~0.1 Å, there is no evidence for a splitting in the 1.8-2.7 Å region into such narrowly resolvable interatomic distances. Therefore this region of $T(r)$ was obtained by Fourier transformation with the Lorch modification function, virtually eliminating termination ripples, but at the cost of some increase in real-space resolution.

Magnesium is the smallest of the modifier cations in this study, and the Mg-O peak in $T(r)$ for MgP_2O_6 is well separated from the O…O peak and the P-O peaks (Fig. 7a). Contrastingly, for all the other samples studied there is significant overlap between the M-O and O…O peaks. Thus $T(r)$ for MgP_2O_6 provides both a clear measurement of the Mg-O coordination, and a clear measurement of the O…O peak that can be used to aid the interpretation of the results for the other binary metaphosphate samples.

The Mg-O peak in $T(r)$ for MgP_2O_6 shows a clear asymmetry, with an extended tail on the long distance side, and hence it was fitted using two single distance peaks, with the parameters given in Table 6. Note that these two peaks are merely a convenient way of parameterising the distribution of Mg-O distances, and are not evidence of two discrete Mg-O bond lengths. The large error on the total Mg-O coordination number from the fit, 5.0±0.7, arises from the uncertainty of apportioning area between the two peak fit components, and is an over-estimate. Integration of the correlation function from 1.76 to 2.25 Å yields a Mg-O coordination number of 4.76±0.02 and a mean bond length of 2.001 Å, but provides no information on the distribution of distances. Integration gives an underestimate of the value of n_{MgO}, because the high *r* tail of the Mg-O distribution is not included. The difference between the two values for n_{MgO} can be taken as a realistic upper bound on the error in the coordination number, leading to a final result n_{MgO}=5.0(2). There is a number of previous diffraction studies of MgP_2O_6 glass in the literature [74-79]; the earlier reports do not have sufficient real-space resolution to reveal the asymmetry of the Mg-O peak, but it has been noted in the later reports [77-79], which have better resolution. The earlier reports with a symmetric distribution of Mg-O distances reported smaller coordination numbers ranging from 4.0 to 4.6, whereas the later reports with an asymmetric distribution reported larger coordination numbers ranging from 5.3 to 6.3. However, none of the previous reports had a value of Q_{max} as high as in the present study, and this is the first time that MgP_2O_6 glass has been measured with sufficient resolution that there is insignificant overlap between the Mg-O and O…O peaks in $T(r)$; Fig.7 shows the best resolved measurement of the Mg-O peak that has yet been made.

It is most common in crystalline structures for Mg to be octahedrally coordinated by oxygen, and hence the measured coordination number of 5.0(2) is surprisingly low. For example, in crystalline $Mg_2P_4O_{12}$ there are two Mg sites and both are octahedral [80]. Fig. 11a shows a comparison of $T(r)$ for MgP_2O_6 glass with a simulation for crystalline $Mg_2P_4O_{12}$, produced by use of the XTAL program [81,82]. The simulated P-O, Mg-O and O…O peaks were broadened using the same values for the variation in bond length as obtained for the fits to $T(r)$ for the glass (Tables 5 and 6). There is a close similarity between the two P-O peaks at ~1.5 Å, since both glass and crystal are formed of PO_4 tetrahedra. However, there is a marked difference between the two Mg-O peaks at ~2.0 Å; for the glass the Mg-O peak is shifted to shorter distance and has smaller area. These differences are what is

expected for a smaller coordination number in the glass, since bond valence consideration shows a strong correlation between coordination number and bond length [83,84]. It is of note that studies of magnesium silicate glasses also find an asymmetric distribution of Mg-O distances [85], and coordination numbers less than 6. In particular, the Mg-O coordination number in magnesium metasilicate glass, $MgSiO_3$, has been measured using neutron diffraction with isotopic substitution to be 4.5(1), with fitted bond lengths of 1.997 Å and 2.21 Å [86]. Comparison of our measurement of $T(r)$ for MgP_2O_6 glass with the previous measurements that observed the asymmetric Mg-O distribution shows that they have over-estimated the extent to which the Mg-O distribution continues underneath the O…O peak in $T(r)$, due to insufficient resolution to clearly resolve the Mg-O and O…O peaks. This is the reason why they have obtained higher values for the coordination number. Table 6 gives a calculation of the bond valence for the two fitted peaks [83,84], and their sum is very close to the ideal value of two (the formal valence of Mg^{2+}), indicating that the observed distribution of Mg-O coordination is a reasonable measurement. Finally, it is important to note that even though the Mg-O coordination number is low, 5.0(2), the NMR results indicate that MgO acts as a network modifier, not as a network former.

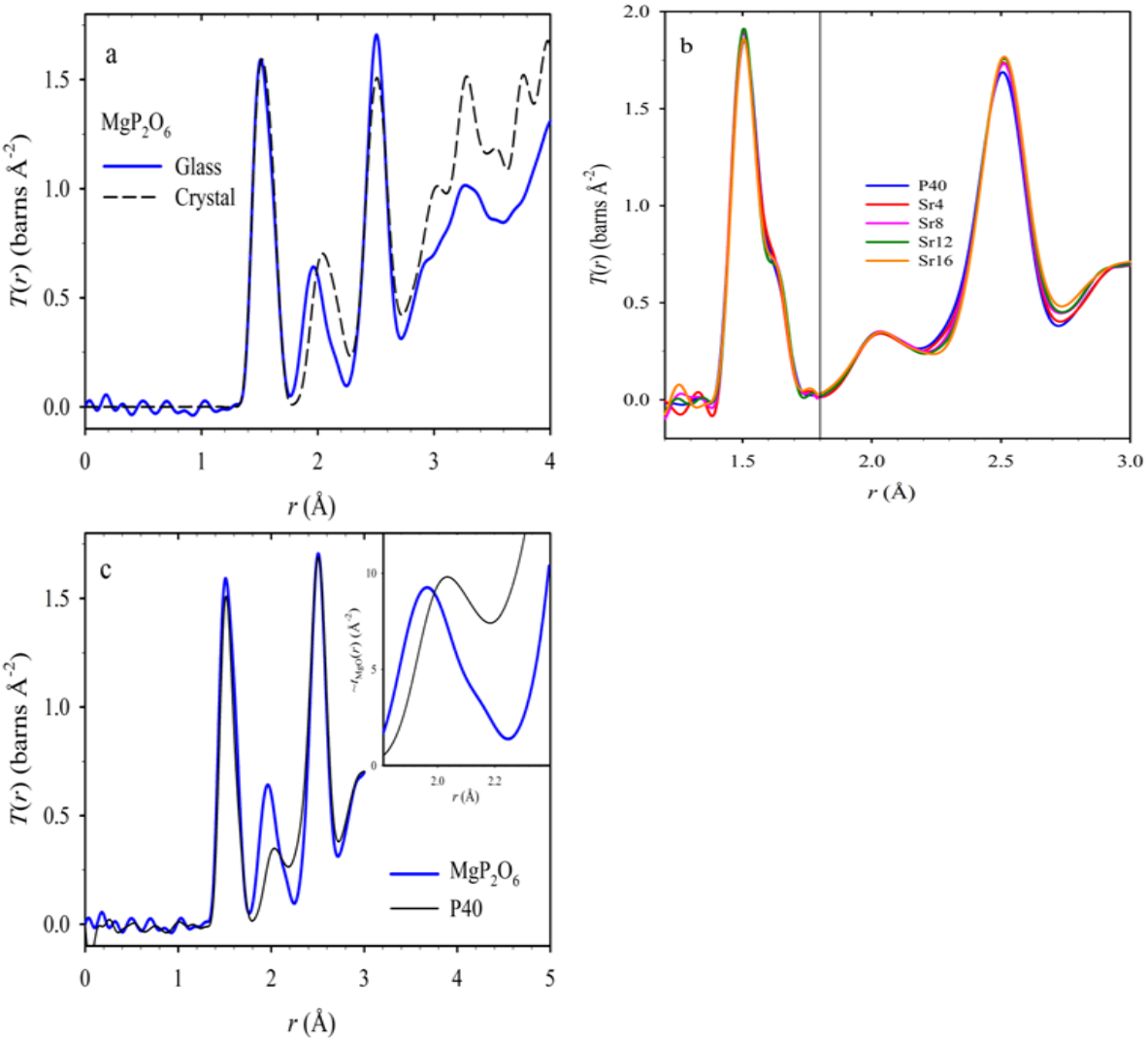

Fig. 11 Comparisons between various total correlation functions, $T(r)$, evaluated using only the Lorch modification function [48], unless stated otherwise. a) MgP_2O_6 glass (blue, continuous line) compared with a simulation for crystalline $Mg_2P_4O_{12}$ [80] (black, dashed line). b) Comparison of multicomponent glasses evaluated using the step modification function for distances shorter than 1.8 Å. c) MgP_2O_6 glass (blue, thick line) compared with P40 glass (black, thin line). The inset shows the two correlation functions in the region of the Mg-O peak, after division by the Mg-O coefficient (Eqn. 3) so as to yield the Mg-O partial correlation function, $t_{\mathrm{MgO}}(r)$.

Table 6: The M-O (and O…O) parameters from fitting the correlation functions, $T(r)$, of the binary metaphosphate glasses, and the multicomponent Sr-series glasses. See the text for details of the fitting. The valence calculated from the parameters for M-O bonds is also given.

Sample	**Atom pair $l-l'$**	**Bond length ($r_{ll'}$/Å)**	**Bond length variation ($\langle u_{ll'}^2\rangle^{½}$/Å)**	**Coordination number ($n_{ll'}$)**	**M-O valence (*e*)**
MgP_2O_6	Mg-O	1.945 (1)	0.066 (4)	2.6 (5)	1.30
	Mg-O	2.07 (3)	0.11 (1)	2.4 (5)	0.87
	Mg-O sum			**5.0 (7)**	**2.17**
	O…O	2.5059 (9)	0.084 (1)	4.29 (4)	
CaP_2O_6	Ca-O	2.299 (2)	0.078 (2)	2.91 (6)	1.19
	Ca-O	2.506 (2)	0.069 (2)	2.10 (7)	0.49
	Ca-O sum			**5.01 (9)**	**1.68**
SrP_2O_6	Sr-O	2.559 (1)	0.111 (1)	5.10 (6)	1.55
$Na_2P_2O_6$	Na-O	2.284 (2)	0.100 (3)	2.58 (6)	0.70
	Na-O	2.564 (3)	0.070 (5)	1.20 (7)	0.15
	Na-O sum			**3.77 (9)**	**0.85**
Multicomponent Sr-series glasses	Mg-O	2.01	0.09	2.77	1.18
	Mg-O	2.06	0.09	2.19	0.81
	Mg-O sum			**4.96**	**1.99**
	O…O	2.51	0.09	4.25	

The peak at *ca.* 2.5 Å in $T(r)$ for MgP_2O_6 glass was fitted by a single peak with the parameters given in Table 6. The average O…O coordination number for the O…O distance in a PO_4 unit in an alkali or alkaline earth phosphate glass with 100*y* mol% P_2O_5 is given by

$$n_{\mathrm{OO}} = 3n_{\mathrm{OP}} = \frac{24y}{1+4y} \qquad (6)$$

and thus for the metaphosphate composition (*y*=0.5) a value n_{OO}=4 is expected. The O…O coordination number, n_{OO}=4.29(4), from the fit is larger than this value, and the discrepancy is also apparent from the glass/crystal comparison shown in Fig.8. In the crystal there are only O…O distances in the range ~2.25 Å – 2.7 Å, and the discrepancy is evidence that in the glass there are also a small number of other types of distance in this range. It is most probable that the extra contribution in this distance range is due to cation-cation pairs, perhaps P-P pairs with small P-Ô-P bond angles ~110°.

Whereas the Mg-O peak in $T(r)$ for MgP_2O_6 is well separated from the O…O peak, for the other binary metaphosphates the M-O peak (M=Ca, Sr, Na) overlaps to a large extent with the O…O peak, and thus the distributions of M-O distances cannot be determined by direct fitting of $T(r)$. However, since the metaphosphate samples all have the same stoichiometry, it is reasonable to assume that the O…O peak is very similar for all of them. Therefore, the O…O peak that was fitted to $T(r)$ for MgP_2O_6 was subtracted from $T(r)$ for each of the other binary metaphosphates, and then the residual was fitted to yield an estimate of the M-O distribution. $Na_2P_2O_6$ has a different oxygen

atomic fraction, c_O, to the alkaline earth metaphosphates, and hence for this sample the O…O peak was multiplied by 0.9 prior to the subtraction (see Eqn. 3). The parameters for the peaks fitted to the M-O distributions are given in Table 6, together with a bond-valence [83,84] calculation of the valence of the M-O bonds. The valence sums are reasonable but are not as close to the ideal values (the formal valence of the M cation) as is the case for the Mg-O peak fit; this is perhaps to be expected because the fits are derived from a region of $T(r)$ that is dominated by the O…O contribution.

The Ca-O distribution in CaP_2O_6 is asymmetric and was fitted by two peaks, similar in form to the Mg-O distribution, but with a greater spread in distances. The total Ca-O coordination number of 5.01 for the glass is relatively small compared to the average value of 7.5 for crystalline β-$Ca(PO_3)_2$ [87], but the crystal has a much longer average Ca-O bond length of 2.47 Å compared to the average value of 2.38 Å for the fit reported in Table 6, and so the result may be reasonable. In a combined neutron and X-ray diffraction study of calcium metaphosphate glass, Wetherall *et al*. [44] have found a Ca-O coordination of 5.2 at a distance of 2.35 Å, similar to our result, and also additional coordination of 1.7 at a distance of 2.86 Å, beyond the range that we have addressed.

Our fit to the Sr-O distribution in SrP_2O_6 consists of a single peak at a distance of 2.559 Å. Martin *et al*. [23] have found evidence for an asymmetric distribution of Sr-O distances in silicate glass, and it is likely that there is also an additional Sr-O component at longer distance in metaphosphate glass, as for Mg-O and Ca-O, but this is beyond the range that we have been able to probe. The measured Sr-O coordination number of 5.96 for the glass is smaller than the value of 8.0 for crystalline γ-$Sr(PO_3)_2$ [88], but the crystal has a longer average bond length of 2.65 Å, and so it is expected to have a larger coordination number. In a high energy X-ray diffraction study of strontium metaphosphate glass, Hoppe *et al*. [89] have determined a Sr-O coordination number and bond length of 6.0 and 2.552 Å, very similar to those reported here.

The Na-O distribution in $Na_2P_2O_6$ is asymmetric and was fitted by two peaks, as for the Mg-O and Ca-O distributions, but with an even greater spread in distances. The measured Na-O coordination number of 3.77 is smaller than the value of 5.0 for crystalline α-$NaPO_3$ [90], but the crystal has a longer average bond length, 2.43 Å, compared to the average for the glass, 2.36 Å, and so the crystal should be expected to have a larger coordination number. In a neutron diffraction study of sodium metaphosphate glass, Pickup *et al*. [37] found a Na-O coordination number of 4.0 at a single distance of 2.33 Å, whilst in a combined neutron and X-ray diffraction study Hoppe *et al*. [91] found an asymmetric distribution of Na-O distances with a total coordination number of 4.20.

In summary, we have found that in binary metaphosphate glasses M-O (M=Mg, Ca, Sr, Na) coordination numbers are smaller and M-O bond lengths are shorter than in corresponding crystals. The distributions of M-O bond lengths are broad and asymmetric.

4.4.4 Modifier coordination in multicomponent glasses

For the multicomponent glasses, the region of $T(r)$ from *ca.* 1.8 Å to *ca.* 2.7 Å cannot be deconvoluted using the same fitting procedure as for the binary glasses because there are too many overlapping contributions (for Sr4, Sr8 and Sr12 there are contributions from Mg-O, Na-O, Ca-O, Sr-O

and O…O pairs). Fig. 11b shows a comparison of $T(r)$ for the five Sr-series multicomponent glasses, showing a great deal of similarity. Nevertheless, as Sr substitutes for Ca, there are small differences either side of the major peak at ~2.5Å, consistent with the loss of the Ca-O contribution at shorter distances and the growth of the Sr-O contribution at longer distances. Fig. 11c shows a comparison of $T(r)$ for MgP_2O_6 and P40, and there is a marked difference in the clearly resolved Mg-O peak at *ca.* 2.0 Å. As shown by Eqn. 3, the Mg-O contribution is weighted by the Mg atomic fraction, c_{Mg}, and this is why the Mg-O peak for P40 (24 mol% MgO) has roughly half the size of the peak for MgP_2O_6 (50 mol% MgO). However, the inset to Fig. 11c shows the region around the Mg-O peak after division by the factor $2c_{\mathrm{Mg}}\bar{b}_{\mathrm{Mg}}\bar{b}_{\mathrm{O}}$, so as to yield the Mg-O partial correlation function, $t_{\mathrm{MgO}}(r)$. This inset shows that for P40 the Mg-O distribution is shifted significantly to longer bond length. In a neutron diffraction study of three magnesium phosphate glasses of different composition, Suzuya *et al*. [78] have also observed composition-dependent changes in the distribution of Mg-O distances.

Fig. 11b shows that for the Sr-series, $T(r)$ is almost exactly the same, and the only small identifiable differences are consistent with the substitution of Sr for Ca. That is to say, the substitution of Sr for Ca causes a loss of area in the region of the Ca-O distribution (*r*~2.15-2.40 Å), and a growth in area in the region of the Sr-O distribution (*r*~2.45-2.95 Å). Therefore, a fitting approach was adopted for the Sr-series in which it is assumed that the coordination of each modifier ion is the same in all of the samples, *i.e*. the M-O coordination number and distribution of M-O bond lengths remains the same, independent of SrO content. In this approach, the correlation functions of *all five* multicomponent Sr-series glasses were fitted *simultaneously*, with one single set of parameters ($r_{ll'}$, $\langle u_{ll'}^2\rangle^{½}$and $n_{ll'}$) to describe each coordination, as given in Table 6. This was achieved by use of a specially developed version of the programme NXFit [92], which also takes into account the correct real-space resolution function (as for PFIT) [71,72], but does not evaluate errors on the fitted parameters. For Ca-O, Sr-O and Na-O, the parameters ($n_{ll'}$, $r_{ll'}$, and $\langle u_{ll'}^2\rangle^{½}$) were fixed at the values found for the binary metaphosphates (Table 6), because no evidence has been found for a change. On the other hand, Fig. 11c shows clear evidence for a marked change in the Mg-O parameters, and hence these were allowed to vary in the fit. Also the parameters for the O…O peak were allowed to vary, and the P-O peak was included in the fit so as to take into account the small overlap with the Mg-O peak. The correlation functions obtained using the Lorch modification function were fitted in this fitting procedure over the range of 1.5 to 2.65 Å. The fitted functions are shown in Fig. 12, and the final entry of Table 6 gives the parameters obtained. The fits to the modifier-oxygen contributions as shown in Fig. 12 are satisfactory, although the residual for the Sr16 glass between 2.2 and 2.7 Å is noisier than for the others.

These fitting results show that the measured correlation functions for the Sr-series are consistent with a structural model in which the coordination of the modifiers does not change as Sr is substituted for Ca. Furthermore, the evidence is consistent with a model in which the Ca-O, Sr-O and Na-O coordinations are the same as in binary metaphosphate glasses. The exception is Mg-O; the measured correlation functions are consistent with a model in which the Mg-O coordination does not change for the Sr-series, but is different to that in magnesium metaphosphate glass or crystal. Our results show that for the Sr-series (with 40 mol% P_2O_5) the Mg-O distribution is shifted to longer bond length compared to binary magnesium metaphosphate (50 mol% P_2O_5), but with only a small increase in coordination number. In a neutron diffraction study of binary magnesium phosphate glasses, Suzuya *et al*. [78] also found that the Mg-O distribution for 40 mol% P_2O_5 is at longer

distance than for 50 mol% P_2O_5, but with little change in coordination number. Also Karakassides *et al*. [93] have reported molecular dynamics calculation for three magnesium phosphate glass compositions, predicting a Mg-O coordination number of five for all compositions, but with a small shift to longer Mg-O distance as the MgO content increases. Thus our result is consistent with the literature.

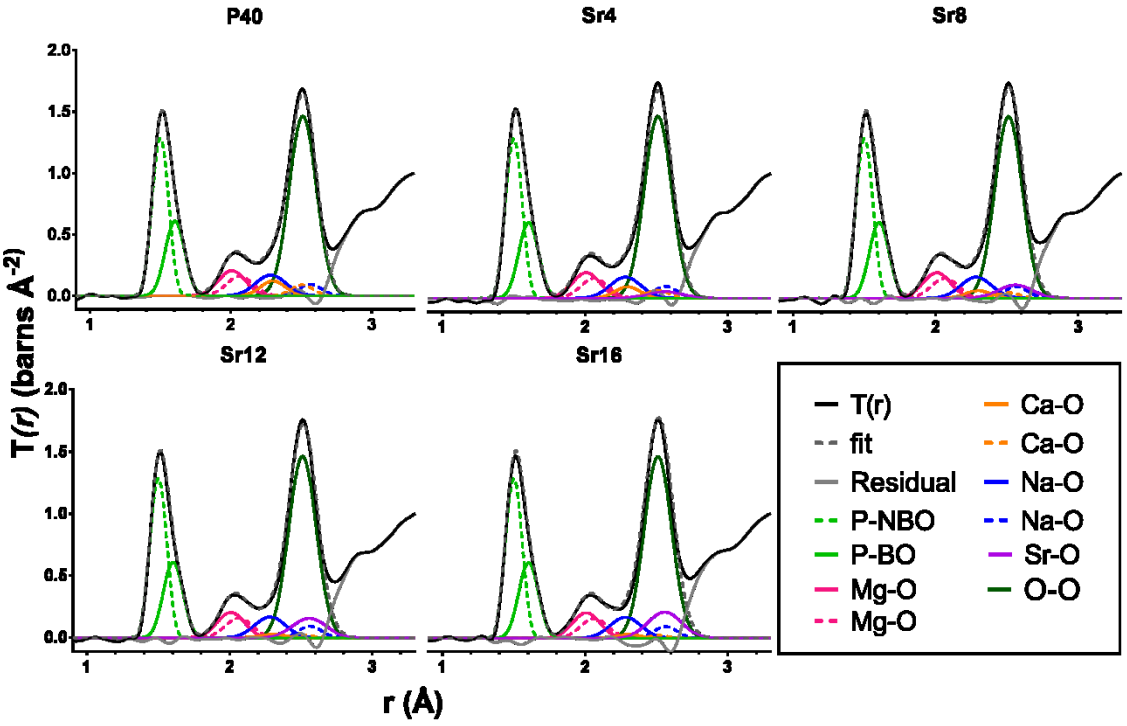

Fig. 12 Total correlation functions, $T(r)$, of multicomponent glasses, together with the results obtained by simultaneously fitting all five functions simultaneously using a specially developed version of the programme NXFit [92]. See text for details of the fitting, and see legend for explanation of the various lines.

4.4.5 Mg-O coordination in multicomponent glasses

The fact that a simultaneous fit can be made (using the NXfit programme) to the total correlation functions, $T(r)$, of all five multicomponent glasses shows that to a good approximation, the M-O coordinations are the same in all five samples. Furthermore, the Na-O, Ca-O and Sr-O coordinations in the multicomponent glasses are shown to be the same or very similar to those in the binary metaphosphate glasses. The exception to this is the Mg-O coordination, which changes with glass composition. Therefore, a further analysis of the correlation functions was made, in which the P-O, Na-O, Ca-O and Sr-O peaks were subtracted from $T(r)$ for each multicomponent glass to yield a difference function, $\Delta T(r)$, as shown in Fig. 13 for samples P40 and Sr16. For this subtraction, the P-O peaks fitted to $T(r)$ for the multicomponent glass (see section 3.5.2) were used, whilst the Na-O, Ca-O and Sr-O peaks were determined using the parameters from fitting the binary metaphosphate glasses. The difference function, $\Delta T(r)$, has a peak at ~2.03 Å due to Mg-O bonds, and a peak at ~ 2.51 Å due mainly to O…O distances. As Sr substitutes for Ca, the Mg-O peak increases in width

and area. This may be the reason for the noisier residual noted above for the Sr-rich compositions, especially Sr16.

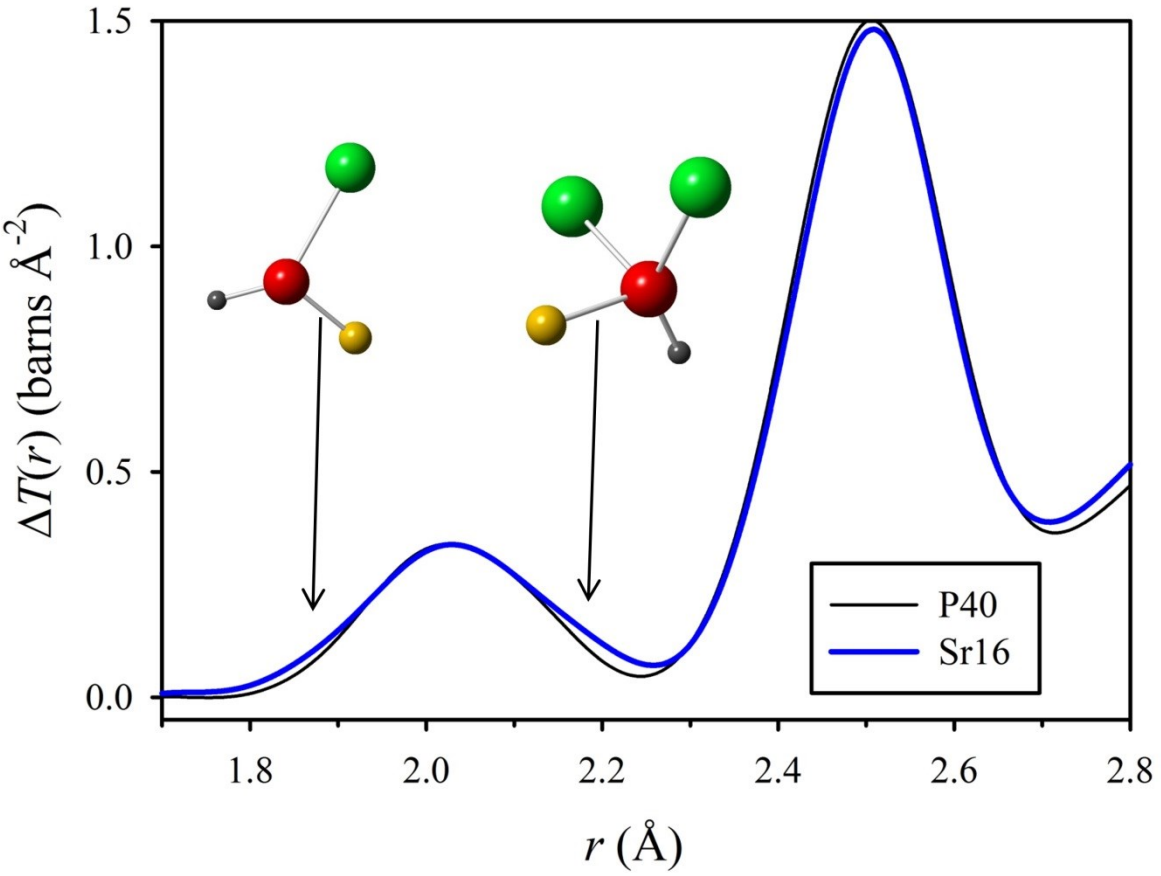

Fig. 13 The correlation functions of the multicomponent glasses P40 and Sr16, after subtraction of the P-O, Na-O, Ca-O and Sr-O peaks; see the text for details. Also shown are examples of atomic environments giving rise to shorter and longer Mg-O bonds. The central (red) atom is a NBO, bonded to one phosphorus (small sphere), one Mg atom (intermediate size sphere), and either one or two other modifier cations (e.g. Sr, large spheres).

The difference functions for the five multicomponent glasses were fitted using two peaks to represent Mg-O and O…O distances respectively (in this case, two Mg-O components were not found to be required or supported by the experimental data), leading to the parameters given in Table 7. The dependence of the parameters on the Ca/Sr substitution is shown in Fig. 14. There is very little change in the fitted parameters for the O…O peak, whilst in contrast there is a small but consistent growth in the Mg-O coordination number, mean Mg-O bond length, and variation in Mg-O bond length, as Sr substitutes for Ca.

It may be understood how the addition of Sr affects the Mg-O bonds, by consideration of the environments of the oxygens bonded to Mg^{2+} cations. Firstly, we note that it is NBOs that are important for this consideration, not BOs. The glass certainly must have Mg-BO bonds, but these BOs are likely to have OP_2Mg motifs [84]; thus these BOs are not bonded to other (non-Mg) modifier cations, and hence the substitution of Sr for Ca does not affect the length of the Mg-BO bonds. A consideration of the electrostatic bond strengths [84] of the various bonds in the glasses shows that

the two most likely motifs for NBOs that are bonded to Mg^{2+} cations are OPMgM and $OPMgM_2$ (where M=Na, Ca or Sr). This conclusion is confirmed by the crystal structure of $SrMgP_2O_7$ [94], in which each Mg-O bond involves an NBO with one of these two motifs. Secondly, we note that Sr^{2+} is the largest modifier cation in these glasses, and hence Sr-O bonds have less valence and are weaker than any of the other M-O bonds. The effect of substituting Sr for Ca in a OPMgM motif will thus be to increase the valence of the Mg-NBO bond, and hence to shorten this bond. This is why the distribution of Mg-O bond lengths extends to shorter distance when Sr substitutes for Ca. On the other hand, the longer Mg-O bonds occur for oxygens with an $OPMgM_2$ motif, and the Sr/Ca substitution has a different effect on these motifs: The electrostatic bond strength of M-O bonds for M=Ca is ~0.4 (based on a Ca-O coordination number of five – see Table 6), so that the bond strength sum is considerably in excess of two for an oxygen with an $OPMgCa_2$ motif. This means that $OPMgCa_2$ motifs are not very likely to occur. However, if Sr substitutes for Ca, then the bond strength sum for the $OPMgM_2$ motif is decreased closer to two, and hence the motif is more likely to occur. Thus the substitution of Sr for Ca leads to a growth in the number of $OPMgM_2$ motifs, and this is why the substitution leads to a growth in the long distance part of the distribution of Mg-O bond lengths. The two types of NBO motif giving rise to the short Mg-O bonds and the long Mg-O bonds, as in crystalline $SrMgP_2O_7$ [94], are illustrated in Fig. 13. The growth in the coordination number n_{MgO} suggests that the growth in $OPMgM_2$ motifs is the dominant effect on Ca/Sr substitution.

Table 7: The Mg-O (and O…O) parameters from fitting the correlation functions, $\Delta T(r)$, of the multicomponent Sr-series glasses, after subtraction of the P-O, Na-O, Ca-O and Sr-O peaks; see the text for details. The valence calculated from the parameters for Mg-O bonds is also given.

Sample	**Atom pair $l - l'$**	**Interatomic distance ($r_{ll'}$/Å)**	**Variation in interatomic distance ($\langle u_{ll'}^2 \rangle^{½}$/Å)**	**Coordination number ($n_{ll'}$)**	**Mg-O valence (e)**
P40	Mg-O O…O	2.0325 (5) 2.5063 (2)	0.0083 (6) 0.0833 (2)	4.73 (2) 4.13 (1)	1.89
Sr4	Mg-O O…O	2.0344 (6) 2.5082 (2)	0.0891 (7) 0.0813 (2)	4.62(3) 4.10 (1)	1.84
Sr8	Mg-O O…O	2.0353 (6) 2.5073 (2)	0.0926 (7) 0.0816 (2)	4.94 (3) 4.03 (1)	1.96
Sr12	Mg-O O…O	2.0358 (6) 2.5080 (2)	0.0940 (7) 0.0815 (2)	4.92 (3) 4.04 (1)	1.95
Sr16	Mg-O O…O	2.0365 (7) 2.5073 (2)	0.1021 (7) 0.0814 (2)	5.20 (3) 3.97 (1)	2.05

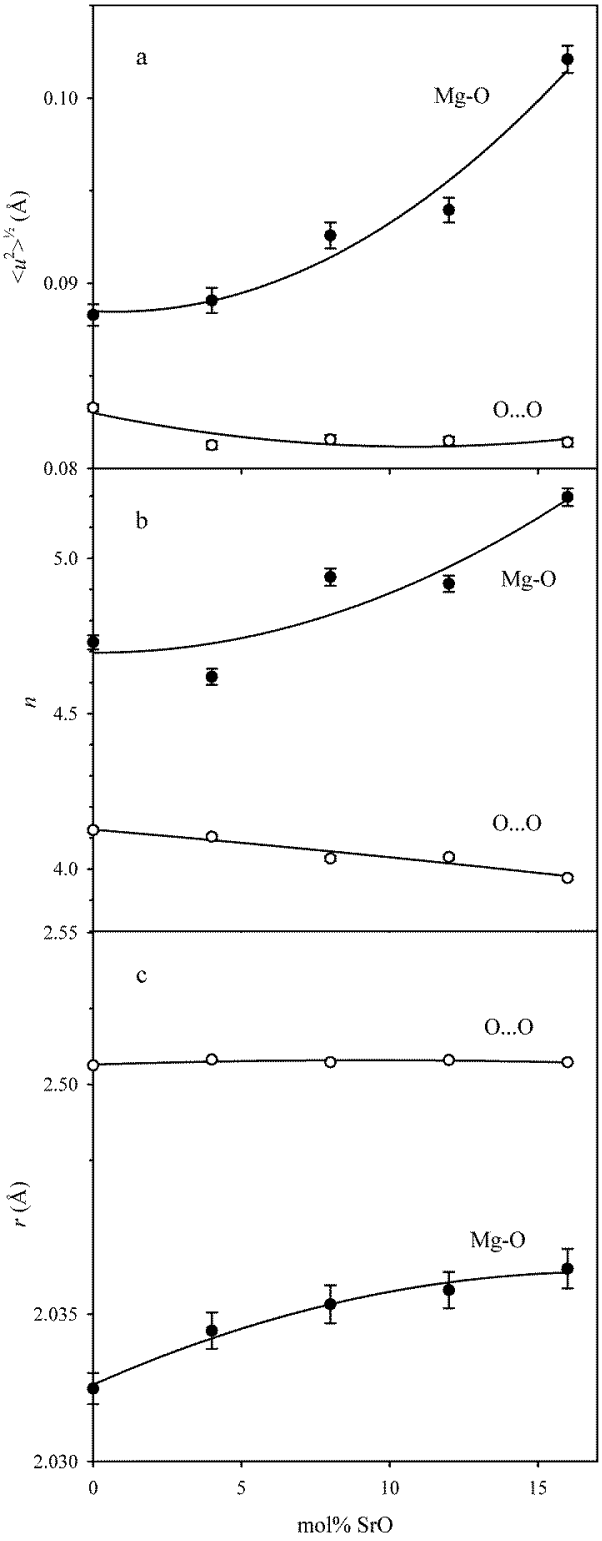

Fig. 14 The Mg-O (closed symbols) and O…O (open symbols) parameters for peak fits to the correlation functions, $\Delta T(r)$, of the multicomponent Sr-series glasses, after subtraction of the P-O, Na-O, Ca-O and Sr-O peaks; see the text for details of the subtraction. The lines are guides to the

eye. a) The RMS variation in distance ($\left\langle u^2_{\mathrm{MgO}} \right\rangle^{½}$ and $\left\langle u^2_{\mathrm{O\ldots O}} \right\rangle^{½}$, a measure of the peak width), b) the coordination number (n_{MgO} and $n_{\mathrm{O\ldots O}}$), and c) the mean interatomic distance (r_{MgO} and $r_{\mathrm{O\ldots O}}$).

4.5. Dissolution and ion release

The pH values shown in Fig. 8 remain around 7 for all compositions. This is expected for glass compositions that are classed as invert, and has been seen previously where a neutral pH was maintained during dissolution as opposed to acidic pH values seen with metaphosphate compositions [95,96]. The stable, neutral pH observed throughout this dissolution study suggests that the dissolution mechanism was again controlled predominantly by the modifier ion–phosphate chain interaction and network connectivity, rather than the surrounding solution.

It is well known that the physical-chemical properties of phosphate glasses are largely dependent on the cations that modify the network. These cations are thought to take up the interstitial sites created between phosphate chains, increasing the resistance to hydrolysis [38]. As mentioned previously, the field strength of Sr^{2+} is less than that of Ca^{2+} (as a result of the larger ionic radius), and thus it may be hypothesised that the dissolution rate of the higher SrO containing glasses would be greater than those with more CaO. However, this is not what was found. The initial addition of SrO to the glass (adding 4 mol% SrO) caused a reduction in the dissolution rate as shown in Fig. 9, suggesting that replacing Ca with Sr can increase cross-linking between phosphate chains. The average mass loss per unit area decreased significantly ($P < 0.001$) on addition of 4 mol% strontium oxide from 8.4×10^{-4} g cm^{-2} to 5.5×10^{-4} g cm^{-2} at 72 hours (see Fig. 9). However, further substitution of Sr for Ca had no significant effect on either average mass loss per unit area or dissolution rate for the mixed Sr/Ca compositions. Nevertheless, for the Ca-free glass Sr16, the mass loss increased slightly. The inset in Fig. 9 shows the dissolution rates for the multicomponent glasses determined via the slope of best fit for each composition in all three media tested. The rate remained similar for all the mixed Sr/Ca glasses, with the greatest change in rate occurring between P40 and Sr4 by 3×10^{-6} g/cm^2/hrs in ultra-pure water, whilst there was a modest increase in rate for Sr16. The same trend was observed in both deionised water and PBS, with P40 degrading at a faster rate than the Sr glasses. A number of studies investigating the dissolution profiles of Sr-containing phosphate glasses have reported that they degrade faster than Sr-free glasses. However, it should be noted that these studies investigated glasses with fixed P_2O_5 content of 50 mol% [57,58,97]. The increased dissolution profiles observed were attributed to expansion of the glass network with the addition of Sr, correlating with an increase in molar volume. However, although a small increase in molar volume (~2%) was seen in this study, it did not exert any influence on the degradation of these glasses with fixed 40 mol% P_2O_5 (i.e. almost invert glass structure).

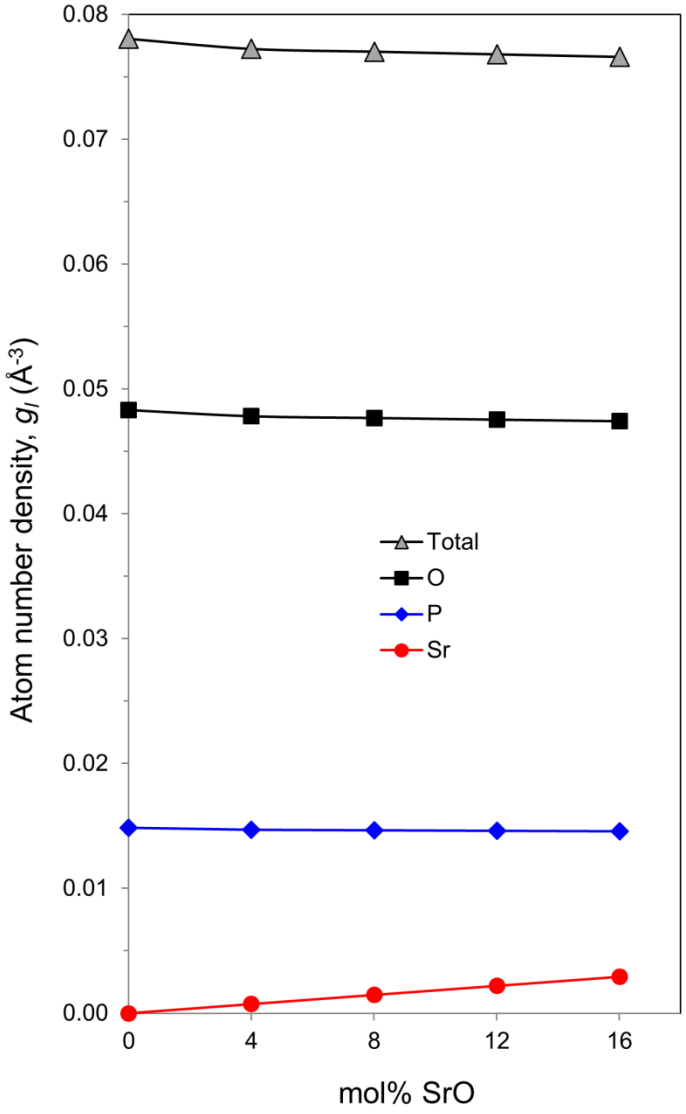

Fig. 15 The total atom number density, and the partial atom number densities for oxygen, phosphorus and strontium in the multicomponent glasses.

Some authors advocate the consideration of oxygen density as being useful for an understanding of the dissolution properties of glasses [53,98], and therefore we show the total atom number density, g_{tot}, and the partial atom number density [99], $g_l = c_l g_{\mathrm{tot}}$, for O, P and Sr in Fig. 15. The number densities of O and P fall steadily by ~2% as Sr substitutes for Ca (the same as the factor by which the molar volume grows). The behaviour of the oxygen number density, g_{O}, does not correlate with the dissolution behaviour shown in Fig. 9. *i.e.* g_{O} shows a steady slight fall, whereas the mass loss is higher for the samples P40 and Sr16, but lower for the intermediate samples. Therefore we conclude that the oxygen density does not provide any direct explanation for the observed dissolution behaviour.

The dissolution rates of the Sr-containing glass in this study did not vary greatly in any of the media tested. One explanation for this could be due to the fact that these glasses are on the verge of being an invert glass, and the various glass properties (e.g. dissolution rate) of such glasses are not controlled by the glass (P_2O_5) network skeleton nor the entanglement of chains, but rather the

interaction of cations with the phosphate groups [27,35,96,100]. The total Ca-O and Sr-O coordination numbers reported in Table 6 are both close to five. However, there is a major difference between these two results, in that the Ca-O value includes a significant contribution from a long distance tail in the distribution, whereas the long distance tail has not been taken into account for the Sr-O value, because it is at too long a distance to be readily accessible. Thus it is most likely that the total Sr-O coordination number is significantly in excess of five. This suggests in turn that the decrease in dissolution rate for Sr-containing glasses could be attributed to the increase in coordination number leading to a more highly cross-linked structure, with increased resistance to hydrolysis. Alternatively, it is notable that the dissolution rate shown in Fig. 9 is higher for the two samples (P40 and Sr16) that contain four oxide components, whereas the samples with five components have a dissolution rate that is lower and is constant; this observation suggests that the greater structural frustration arising from the larger number of glass components leads to a smaller dissolution rate. It is also of note that the Sr16 sample is more prone to crystallisation than the other multicomponent samples (note the low values of T_{onset} and T_c in Table 2), suggesting that the greater frustration of the 5-component samples gives them a greater resistance to crystallisation.

Alternatively, the way in which the dissolution rate (Fig. 9) is lower for the mixed Sr/Ca compositions compared to the rate for the single cation glasses (P40 and Sr16) suggests a mixed mobile ion (MMI) effect [101]. The temperatures T_c and T_{onset} also show a behaviour of this type, with higher values for the mixed Sr/Ca glasses, and lower values for the single cation glasses. Furthermore the Na^+ and Mg^{2+} cation release rates (Fig. 10) show this MMI effect type of behaviour. According to this viewpoint, the dissolution rate for mixed Sr/Ca glasses is lower than for single cation glasses because Sr hinders motion of Ca and vice versa, similar to the way in which mixed alkali glasses have lower conductivities than single alkali glasses [102,103].

Furthermore, the compositions studied here had high concentrations of MgO present where Mg^{2+} has an even higher field strength (0.53 valence/$Å^2$ when 4-coordinated or 0.46 valence/$Å^2$ when 6-coordinated) than Ca^{2+} and Sr^{2+} due to the increasing atomic number of the alkaline earth metals [62]. This in turn would increase packing density and so decrease dissolution and hence ion release rates. According to Dietzel's rule [60,61], MgO is also known to behave as an intermediate, acting as either a network modifier or enter the phosphate network forming P-O-Mg bonds. From the ^{31}P NMR results in this study, it was clear the MgO behaved as a glass modifier. Furthermore, the minimal change observed in the dissolution rates between the SrO containing glasses may be attributed to the dominating role MgO can play within the network because the MgO concentration (24mol%) remained constant for each composition. The significant decrease in dissolution rate of SrO containing glasses compared to the Sr free glass (P40) could be attributed to the increased packing density and crosslinking caused with the addition of an extra cation.

The ion release profiles for Na^+ and Mg^{2+} (Fig. 10) follow a similar trend to the dissolution study where P40 released the highest concentration of cations over time, and strontium-containing glasses showed a consistent release of cations ranging from 0.27ppm for Sr4 at 24 hours to 50.95ppm for Sr16 at 672 hours. The correlation of ion release studies of Na^+ and Mg^{2+} have also been observed by Ahmed *et al*. [3] where a cumulative release method was also used for a ternary phosphate glass. It was interesting to note that the concentration of Sr^{2+} released by the Sr 16 glass where CaO was fully substituted with SrO, was greater than the Ca^{2+} released from the P40 samples containing 0 mol% SrO. As expected a gradual increase in SrO in the glass samples resulted in a gradual increase

in the amount of strontium and reduction in calcium ions released. These release profiles of Sr^{2+} coupled with the dissolution rate profiles provided evidence that it was possible to control the concentration of strontium ions released without affecting the rate of dissolution.

The ability to retain both structural and physico-chemical properties of the glasses in this study suggest the possibility of fine tuning the release of therapeutic ions such as Sr. Treatment of osteoporosis has involved oral administration of strontium ranelate at doses of 2g per day [25]. This study has shown that dissolution rates of Sr-containing glasses could be maintained and that a linear rate of change of Sr release has been achieved with varying concentration. This study shows it is possible to preserve the optimised properties of the glass formulation whilst having a predictable release rate of Sr.

5. Conclusions

A comprehensive study of the structure and properties of $40P_2O_5 \cdot (16\text{-}x)CaO \cdot 20Na_2O \cdot 24MgO \cdot xSrO$ glass (x = 0, 4, 8, 12 and 16 mol%) has been described. The substitution of Sr for Ca leads to a slight overall fall in glass transition temperature T_g, and a significant fall in melting temperature, T_m, because Sr-O bonds are weaker than Ca-O bonds, and this effect is more significant than any change in cross-linking of the network. The broadening of the crystallisation peak and the appearance of a second melting event as the SrO content increases are evidence for the formation of more than one crystalline phase. Changes in the crystallisation behaviour are the main factor affecting the width of the thermal processing window for these glasses. FTIR and NMR spectra (^{31}P and ^{23}Na) show no evidence for changes in the phosphate part of the network as Sr substitutes for Ca, and this is confirmed by neutron diffraction results. The ^{31}P NMR spectra show that the multicomponent glasses have equal numbers of PO_4 tetrahedra occurring as Q^2 and Q^1 species, as is expected if all the modifier cations (Mg, Ca, Sr, Na) play the role of network modifiers, not network formers.

Neutron diffraction performed on binary metaphosphate glasses showed that in these glasses the M-O coordinations (M=Mg, Ca, Sr, Na) have a broad asymmetric distribution of bond length, with coordination numbers that are smaller and bond lengths that are shorter than in corresponding crystals. The most reliably determined coordination number is n_{MgO}=5.0(2). The Ca-O and Sr-O coordination numbers were determined as 5.01(9) and 5.10(6), but it is most likely that the Sr-O distribution includes an additional contribution at longer distance, beyond the range that we were able to probe. The neutron correlation functions for the multicomponent glasses are consistent with a structural model in which the coordination of Ca, Sr and Na is the same as in the binary metaphosphate glass. On the other hand, the Mg-O bonds in the multicomponent glasses are shifted to longer distance than for the binary metaphosphate glass. Furthermore, there is a small but consistent increase in the Mg-O coordination number and the width of the distribution of Mg-O bond lengths, as Sr substitutes for Ca.

The glasses with five components have a lower dissolution rate than the four-component glasses, and this may either be due to the increased cross-linking and packing density that arises from the addition of SrO, or simply to the increased structural frustration associated with the larger number of components. The results suggest that phosphate glasses with compositions close to invert formulations (i.e. fixed with 40 mol% P_2O_5) could provide a means of releasing controlled quantities of Sr^{2+} ions without significantly hindering the dissolution rate.

Acknowledgements

The authors would like to acknowledge that the Solid-state NMR spectra were obtained at the EPSRC UK National Solid-state NMR Service at Durham. The authors would also like to acknowledge funding received from the Science and Technology Facilities Council (STFC ref. no. ST/L502583/1).

References

[1] I. Ahmed, M. Lewis, I. Olsen, J.C. Knowles, Phosphate glasses for tissue engineering: Part 1. Processing and characterisation of a ternary-based P_2O_5-CaO-Na_2O glass system, Biomaterials 25 (2004) 491-499.

[2] I. Ahmed, M. Lewis, I. Olsen, J.C. Knowles, Phosphate glasses for tissue engineering: Part 2. Processing and characterisation of a ternary-based P_2O_5-CaO-Na_2O glass fibre system, Biomaterials 25 (2004) 501-507.

[3] I. Ahmed, M.P. Lewis, S.N. Nazhat, J.C. Knowles, Quantification of anion and cation release from a range of ternary phosphate-based glasses with fixed 45 mol% P_2O_5, J. Biomater. Appl. 20 (2005) 65-80.

[4] M.S. Hasan, I. Ahmed, A.J. Parsons, G.S. Walker, C.A. Scotchford, Material characterisation and cytocompatibility assessment of quinternary phosphate glasses, J. Mater. Sci. Mater. Med. 23 (2012) 2531-2541.

[5] N. Sharmin, M.S. Hasan, A.J. Parsons, D. Furniss, C.A. Scotchford, I. Ahmed, C.D. Rudd, Effect of Boron Addition on the Thermal, Degradation, and Cytocompatibility Properties of Phosphate-Based Glasses, BioMed Res. Int. (2013) 902427.

[6] X. Liu, M.N. Rahaman, D.E. Day, In vitro degradation and conversion of melt-derived microfibrous borate (13-93B3) bioactive glass doped with metal ions, J. Am. Ceram. Soc. 97 (2014) 3501-3509.

[7] M. Bitar, V. Salih, V. Mudera, J.C. Knowles, M.P. Lewis, Soluble phosphate glasses: in vitro studies using human cells of hard and soft tissue origin, Biomaterials 25 (2004) 2283-2292.

[8] V. Mouriño, J.P. Cattalini, A.R. Boccaccini, Metallic ions as therapeutic agents in tissue engineering scaffolds: an overview of their biological applications and strategies for new developments, J. R. Soc. Interface 9 (2012) 401-419.

[9] A. Hoppe, V. Mourino, A.R. Boccaccini, Therapeutic inorganic ions in bioactive glasses to enhance bone formation and beyond, Biomater. Sci. 1 (2013) 254-256.

[10] I. Ahmed, A. Parsons, A. Jones, G. Walker, C. Scotchford, C. Rudd, Cytocompatibility and effect of increasing MgO content in a range of quaternary invert phosphate-based glasses, J. Biomater. Appl. 24 (2010) 555-575.

[11] A. Kiani, N.J. Lakhkar, V. Salih, M.E. Smith, J.V. Hanna, R.J. Newport, D.M. Pickup, J.C. Knowles, Titanium-containing bioactive phosphate glasses, Philos. T. R. Soc. A 370 (2012) 1352-1375.

[12] E.A. Abou Neel, I. Ahmed, J.J. Blaker, A. Bismarck, A.R. Boccaccini, M.P. Lewis, S.N. Nazhat, J.C. Knowles, Effect of iron on the surface, degradation and ion release properties of phosphate-based glass fibres, Acta Biomater. 1 (2005) 553-563.
[13] J.R. Jones, A.G. Clare, eds. Bio-Glasses: An Introduction. 2012, Wiley: Chichester.
[14] P.J. Marie, P. Ammann, G. Boivin, C. Rey, Mechanisms of action and therapeuticpotential of strontium in bone, Calcif. Tissue Int. 69 (2001) 121-129.
[15] E. Bonnelye, A. Chabadel, F. Saltel, P. Jurdic, Dual effect of strontium ranelate: Stimulation of osteoblast differentiation and inhibition of osteoclast formation and resorption in vitro, Bone 42 (2008) 129-138.
[16] S.G. Dahl, P. Allain, P.J. Marie, Y. Mauras, G. Boivin, P. Ammann, Y. Tsouderos, P.D. Delmas, C. Christiansen, Incorporation and distribution of strontium in bone, Bone 28 (2001) 446-453.
[17] Y.C. Fredholm, N. Karpukhina, D.S. Brauer, J.R. Jones, R.V. Law, R.G. Hill, Influence of strontium for calcium substitution in bioactive glasses on degradation, ion release and apatite formation, J. R. Soc. Interface 9 (2012) 880-889.
[18] M.D. O'Donnell, P.L. Candarlioglu, C.A. Miller, E. Gentleman, M.M. Stevens, Materials characterisation and cytotoxic assessment of strontium-substituted bioactive glasses for bone regeneration, J. Mater. Chem. 20 (2010) 8934-8941.
[19] E.A. Abou Neel, W. Chrzanowski, D.M. Pickup, L.A. O'Dell, N.J. Mordan, R.J. Newport, M.E. Smith, J.C. Knowles, Structure and properties of strontium-doped phosphate-based glasses, J. R. Soc. Interface 6 (2009) 435-446.
[20] A. Gorustovich, T. Steimetz, R.L. Cabrini, J.M. Porto López, Osteoconductivity of strontium-doped bioactive glass particles, Bone 41 (2007) S4.
[21] E. Gentleman, Y.C. Fredholm, G. Jell, N. Lotfibakhshaiesh, M.D. O'Donnell, R.G. Hill, M.M. Stevens, The effects of strontium-substituted bioactive glasses on osteoblasts and osteoclasts in vitro, Biomaterials 31 (2010) 3949-3956.
[22] K. Fujikura, N. Karpukhina, T. Kasuga, D.S. Brauer, R.G. Hill, R.V. Law, Influence of strontium substitution on structure and crystallisation of Bioglass® 45S5, J. Mater. Chem. 22 (2012) 7395-7402.
[23] R.A. Martin, H.L. Twyman, G.J. Rees, E.R. Barney, R.M. Moss, J.M. Smith, R.G. Hill, G. Cibin, T. Charpentier, M.E. Smith, J.V. Hanna, R.J. Newport, An examination of the calcium and strontium site distribution in bioactive glasses through isomorphic neutron diffraction, X-ray diffraction, EXAFS and multinuclear solid state NMR, J. Mater. Chem. 22 (2012) 22212-22223.
[24] Public Health Service Agency for Toxic Substances and Disease Registry, Toxicological profile for strontium, https://www.atsdr.cdc.gov/toxprofiles/tp159.pdf, (accessed 7/6/2017).
[25] C.T. Price, J.R. Langford, F.A. Liporace, Essential nutrients for bone health and a review of their availability in the average North American diet, Open Orthop. J. 6 (2012) 143-149.
[26] W.E. Cabrera, I. Schrooten, M.E. De Broe, P.C. D'Haese, Strontium and bone, J. Bone Miner. Res. 14 (1999) 661-668.
[27] J.K. Christie, R.I. Ainsworth, N.H. de Leeuw, Investigating structural features which control the dissolution of bioactive phosphate glasses: Beyond the network connectivity, J. Non-Cryst. Solids 432A (2016) 31-34.
[28] R.K. Brow, Review: The Structure of Simple Phosphate Glasses, J. Non-Cryst. Solids 263-264 (2000) 1-28.
[29] W.H. Zachariasen, The atomic arrangement in glass, J. Am. Chem. Soc. 54 (1932) 3841-3851.
[30] I. Elgayar, A.E. Aliev, A.R. Boccaccini, R.G. Hill, Structural analysis of bioactive glasses, J. Non-Cryst. Solids 351 (2005) 173-183.
[31] B.C. Bunker, G.W. Arnold, J.A. Wilder, Phosphate glass dissolution in aqueous solutions, J. Non-Cryst. Solids 64 (1984) 291-316.

[32] T.A. Abrajano Jr, J.K. Bates, C.D. Byers, Aqueous corrosion of natural and nuclear waste glasses I. Comparative rates of hydration in liquid and vapor environments at elevated temperatures, J. Non-Cryst. Solids 84 (1986) 251-257.

[33] H. Gao, T. Tan, D. Wang, Dissolution mechanism and release kinetics of phosphate controlled release glasses in aqueous medium, J. Control. Release 96 (2004) 29-36.

[34] R.A. Martin, H.L. Twyman, G.J. Rees, J.M. Smith, E.R. Barney, M.E. Smith, J.V. Hanna, R.J. Newport, A structural investigation of the alkali metal site distribution within bioactive glass using neutron diffraction and multinuclear solid state NMR, Phys. Chem. Chem. Phys. 14 (2012) 12105-12113.

[35] G. Walter, J. Vogel, U. Hoppe, P. Hartmann, The structure of $CaO\text{-}Na_2O\text{-}MgO\text{-}P_2O_5$ invert glass, J. Non-Cryst. Solids 296 (2001) 212-223.

[36] D.S. Brauer, R.M. Wilson, T. Kasuga, Multicomponent phosphate invert glasses with improved processing, J. Non-Cryst. Solids 358 (2012) 1720-1723.

[37] D.M. Pickup, I. Ahmed, P. Guerry, J.C. Knowles, M.E. Smith, R.J. Newport, The structure of phosphate glass biomaterials from neutron diffraction and ^{31}P nuclear magnetic resonance data, J. Phys.: Condens. Matter 19 (2007) 415116.

[38] A.J. Parsons, I. Ahmed, C.D. Rudd, G.J. Cuello, E. Pellegrini, D. Richard, M.R. Johnson, Neutron scattering and *ab initio* molecular dynamics study of cross-linking in biomedical phosphate glasses, J. Phys.: Condens. Matter 22 (2010) 485403.

[39] U. Hoppe, R. Kranold, D. Stachel, A. Barz, A.C. Hannon, Variation in P-O bonding in phosphate glasses - a neutron diffraction study, Z. Naturforsch. 55a (2000) 369-380.

[40] B.M. Al-Hasni, G. Mountjoy, E. Barney, A complete study of amorphous iron phosphate structure, J. Non-Cryst. Solids 380 (2013) 141-152.

[41] J.M. Smith, S.P. King, E.R. Barney, J.V. Hanna, R.J. Newport, D.M. Pickup, Structural study of $Al_2O_3\text{-}Na_2O\text{-}CaO\text{-}P_2O_5$ bioactive glasses as a function of aluminium content, J. Chem. Phys. 138 (2013) 034501.

[42] R.M. Moss, D.M. Pickup, I. Ahmed, J.C. Knowles, M.E. Smith, R.J. Newport, Structural characteristics of antibacterial bioresorbable phosphate glass, Adv. Funct. Mater. 18 (2008) 634-639.

[43] R.M. Moss, E.A. Abou, D.M. Pickup, H.L. Twyman, R.A. Martin, M.D. Henson, E.R. Barney, A.C. Hannon, J.C. Knowles, R.J. Newport, The effect of zinc and titanium on the structure of calcium-sodium phosphate based glass, J. Non-Cryst. Solids 356 (2010) 1319-1324.

[44] K.M. Wetherall, D.M. Pickup, R.J. Newport, G. Mountjoy, The structure of calcium metaphosphate glass obtained from x-ray and neutron diffraction and reverse Monte Carlo modelling, J. Phys.: Condens. Matter 21 (2009) 035109.

[45] A.C. Hannon, Results on disordered materials from the GEneral Materials diffractometer, GEM, at ISIS, Nucl. Instrum. Meth. A 551 (2005) 88-107.

[46] A.K. Soper, GudrunN and GudrunX : programs for correcting raw neutron and X-ray diffraction data to differential scattering cross section, Rutherford Appleton Laboratory Technical Report RAL-TR-2011-013, 2011.

[47] A.C. Hannon, W.S. Howells, A.K. Soper, ATLAS: A suite of programs for the analysis of time-of-flight neutron diffraction data from liquid and amorphous samples, Inst. Phys. Conf. Ser. 107 (1990) 193-211.

[48] E. Lorch, Neutron diffraction by germania, silica and radiation-damaged silica glasses, J. Phys. C 2 (1969) 229-237.

[49] B.H. Toby, T. Egami, Accuracy of pair distribution function analysis applied to crystalline and non-crystalline materials, Acta Cryst. A 48 (1992) 336-346.

[50] A.R. Jones, R. Winter, G.N. Greaves, I.H. Smith, ^{23}Na, ^{29}Si, and ^{13}C MAS NMR investigation of glass-forming reactions between Na_2CO_3 and SiO_2, J. Phys. Chem B 109 (2005) 23154-23161.

[51] R.K. Brow, R.J. Kirkpatrick, G.L. Turner, The short range structure of sodium phosphate glasses I. MAS NMR studies, J. Non-Cryst. Solids 116 (1990) 39-45.

[52] A.C. Hannon, Neutron diffraction database, http://www.alexhannon.co.uk/, (accessed 7/6/2017).
[53] H. Morikawa, S. Lee, T. Kasuga, D.S. Brauer, Effects of magnesium for calcium substitution in P_2O_5-CaO-TiO_2 glasses, J. Non-Cryst. Solids 380 (2013) 53-59.
[54] I. Ahmed, A.J. Parsons, C.D. Rudd, S.N. Nazhat, J.C. Knowles, P. Guerry, M.E. Smith, Comparison of phosphate-based glasses in the range $50P_2O_5$-(50-*x*)CaO-*x*Na_2O prepared using different precursors, Glass Technol.: Eur. J. Glass Sci. Technol. A 49 (2008) 63-72.
[55] M.A. Qaysi, N.J. Walters, F. Foroutan, G.J. Owens, H.-W. Kim, R. Shah, J.C. Knowles, Strontium- and calcium-containing, titanium-stabilised phosphate-based glasses with prolonged degradation for orthopaedic tissue engineering, J. Biomater. Appl. 30 (2015) 300-310.
[56] R.D. Shannon, Revised effective ionic radii and systematic studies of interatomic distances in halides and chalcogenides, Acta Cryst. A 32 (1976) 751-767.
[57] N.J. Lakhkar, E.A. Abou Neel, V. Salih, J.C. Knowles, Strontium oxide doped quaternary glasses: effect on structure, degradation and cytocompatibility, J. Mater. Sci.: Mater. Med. 20 (2009) 1339-1346.
[58] N. Lakhkar, E.A.A. Neel, V. Salih, J.C. Knowles, Titanium and strontium-doped phosphate glasses as vehicles for strontium ion delivery to cells, J. Biomater. Appl. 25 (2011) 877-893.
[59] J.E. Shelby, Introduction to glass science and technology. 1997, Letchworth: The Royal Society of Chemistry.
[60] A. Dietzel, Die Kationfeldstärken und ihre Beziehungen zu Entglasungsvorgängen, zur Verbindungsbildung und zu den Schmelzpunkten von Silicaten, Z. Elektrochem. 48 (1942) 9-23.
[61] S. Lee, A. Obata, D.S. Brauer, T. Kasuga, Dissolution behavior and cell compatibility of alkali-free MgO-CaO-SrO-TiO_2-P_2O_5 glasses for biomedical applications, Biomedical Glasses 1 (2015) 151-158.
[62] S. Lee, A. Obata, T. Kasuga, Ion release from SrO-CaO-TiO_2-P_2O_5 glasses in Tris buffer solution, J. Ceram. Soc. Japan 117 (2009) 935-938.
[63] P.Y. Shih, J.Y. Ding, S.Y. Lee, ^{31}P MAS-NMR and FTIR analyses on the structure of CuO-containing sodium poly- and meta-phosphate glasses, Mater. Chem. Phys. 80 (2003) 391-396.
[64] R. Oueslati Omrani, A. Kaoutar, A. El Jazouli, S. Krimi, I. Khattech, M. Jemal, J.-J. Videau, M. Couzi, Structural and thermochemical properties of sodium magnesium phosphate glasses, J. Alloys Comp. 632 (2015) 766-771.
[65] Y.M. Moustafa, K. El-Egili, Infrared spectra of sodium phosphate glasses, J. Non-Cryst. Solids 240 (1998) 144-153.
[66] A.M. Efimov, IR fundamental spectra and structure of pyrophosphate glasses along the 2ZnO·P2O5–2Me2O·P2O5 join (Me being Na and Li), J. Non-Cryst. Solids 209 (1997) 209-226.
[67] S. Lee, H. Maeda, A. Obata, K. Ueda, T. Narushima, T. Kasuga, Structures and dissolution behaviors of MgO–CaO–P2O5–Nb2O5 glasses, J. Non-Cryst. Solids 438 (2016) 18-25.
[68] L.N. Ma, Dissolution behavior of phosphate glasses, Ph.D Thesis, Missouri University of Science and Technology, USA, 2014.
[69] S.L. Tagg, R.E. Youngman, J.W. Zwanziger, The structure of sodium tellurite glasses: Sodium cation environments from sodium-23 NMR, J. Phys. Chem. 99 (1995) 5111-5116.
[70] A.C. Wright, Longer range order in single component network glasses?, Phys. Chem. Glasses Eur. J. Glass Sci. Technol. B 49 (2008) 103-117.
[71] A.C. Hannon, PFIT correlation function fitting software, http://www.alexhannon.co.uk/, (accessed 7/6/2017).
[72] A.C. Hannon, Neutron Diffraction Techniques for Structural Studies of Glasses, in: M. Affatigato (Ed.) Modern glass characterization, Wiley, New York, 2015, p. 158-240.

[73] D.I. Grimley, A.C. Wright, R.N. Sinclair, Neutron scattering from vitreous silica IV. Time-of-flight diffraction, J. Non-Cryst. Solids 119 (1990) 49-64.
[74] W. Matz, D. Stachel, E.A. Goremychkin, The structure of alkaline earth metaphosphate glasses investigated by neutron diffraction, J. Non-Cryst. Solids 101 (1988) 80-89.
[75] E. Matsubara, Y. Waseda, M. Ashizuka, E. Ishida, Structural study of binary phosphate glasses with MgO, ZnO, and CaO by X-ray diffraction, J. Non-Cryst. Solids 103 (1988) 117-124.
[76] U. Hoppe, G. Walter, D. Stachel, Untersuchung der Nahordnungsstruktur von Magnesiumphosphat-Gläsern mit der Röntgendiffraktion, Silikattechnik 41 (1990) 227-230.
[77] U. Hoppe, D. Stachel, D. Beyer, The oxygen coordination of metal ions in phosphate and silicate glasses studied by a combination of x-ray and neutron diffraction, Physica Scripta T 57 (1995) 122.
[78] K. Suzuya, D.L. Price, C.K. Loong, S. Kohara, The structure of magnesium phosphate glasses, J. Phys. Chem. Solids 60 (1999) 1457-1460.
[79] U. Hoppe, R. Kranold, A. Barz, D. Stachel, J. Neuefeind, D.A. Keen, Combined neutron and X-ray scattering study of phosphate glasses, J. Non-Cryst. Solids 293 (2001) 158-168.
[80] A.G. Nord, K.B. Lindberg, The crystal structure of magnesium tetrametaphosphate, $Mg_2P_4O_{12}$, Acta Chem. Scand. A 29 (1975) 1-6.
[81] A.C. Hannon, XTAL: A program for calculating interatomic distances and coordination numbers for model structures, Rutherford Appleton Laboratory Report RAL-93-063, 1993.
[82] A.C. Hannon, XTAL structural modelling software, http://www.alexhannon.co.uk/, (accessed 7/6/2017).
[83] N.E. Brese, M. O'Keeffe, Bond-valence parameters for solids, Acta Cryst. B 47 (1991) 192-197.
[84] A.C. Hannon, Bonding and structure in network glasses, J. Non-Cryst. Solids 451 (2016) 56-67.
[85] S. Kohara, K. Suzuya, K. Takeuchi, C.K. Loong, M. Grimsditch, J.K.R. Weber, J.A. Tangeman, T.S. Key, Glass formation at the limit of insufficient network formers, Science 303 (2004) 1649-1652.
[86] L. Cormier, G.J. Cuello, Mg coordination in a $MgSiO_3$ glass using neutron diffraction coupled with isotopic substitution, Phys. Rev. B 83 (2011) 224204.
[87] W. Rothammel, H. Burzlaff, R. Specht, Structure of calcium metaphosphate $Ca(PO_3)_2$, Acta Cryst. C 45 (1989) 551-553.
[88] M. Graia, A. Driss, T. Jouini, Polyphosphates de strontium $Sr(PO_3)_2$ formes β et γ, Acta Cryst. C 55 (1999) 1395-1398.
[89] U. Hoppe, R. Kranold, D. Stachel, J. Neuefeind, Oxygen coordination of modifier cations in metaphosphate glasses probed by high-energy X-ray diffraction, Phosphorus Res. Bull. 10 (1999) 546-551.
[90] A. McAdam, K.H. Jost, B. Beagley, Refinement of the structure of sodium Kurrol salt $(NaPO_3)_x$, type A, Acta Cryst. B 24 (1968) 1621-1622.
[91] U. Hoppe, L. Delevoye, L. Montagne, M.v. Zimmermann, A.C. Hannon, Structure of Nb_2O_5-$NaPO_3$ glasses by X-ray and neutron diffraction, Phys. Chem. Chem. Phys. 15 (2013) 8520-8528.
[92] D. Pickup, R. Moss, R. Newport, NXFit: a program for simultaneously fitting X-ray and neutron diffraction pair-distribution functions to provide optimized structural parameters, J. Appl. Cryst. 47 (2014) 1790-1796.
[93] M.A. Karakassides, A. Saranti, I. Koutselas, Preparation and structural study of binary phosphate glasses with high calcium and/or magnesium content, J. Non-Cryst. Solids 347 (2004) 69-79.
[94] A.A. Tahiri, B.E. Bali, M. Lachkar, R. Ouarsal, P.Y. Zavalij, $SrMgP_2O_7$, Acta Crystallographica Section E 58 (2002) i9-i11.

[95] T. Kasuga, Y. Hosoi, M. Nogami, M. Niinomi, Apatite formation on calcium phosphate invert glasses in simulated body fluid, J. Am. Ceram. Soc. 84 (2001) 450-452.
[96] D.S. Brauer, N. Karpukhina, R.V. Law, R.G. Hill, Effect of TiO_2 addition on structure, solubility and crystallisation of phosphate invert glasses for biomedical applications, J. Non-Cryst. Solids 356 (2010) 2626-2633.
[97] J. Massera, L. Petit, T. Cardinal, J.J. Videau, M. Hupa, L. Hupa, Thermal properties and surface reactivity in simulated body fluid of new strontium ion-containing phosphate glasses, J. Mater. Sci. Mater. Med. 24 (2013) 1407-1416.
[98] N.H. Ray, Composition-property relationships in inorganic oxide glasses, J. Non-Cryst. Solids 15 (1974) 423-434.
[99] O.L.G. Alderman, A.C. Hannon, S. Feller, R. Beanland, D. Holland, The germanate anomaly in alkaline earth germanate glasses, J. Phys. Chem. C 121 (2017) 9462-9479.
[100] J.K. Christie, R.I. Ainsworth, D. Di Tommaso, N.H. de Leeuw, Nanoscale chains control the solubility of phosphate glasses for biomedical applications, J. Phys. Chem B 117 (2013) 10652-10657.
[101] C.T. Moynihan, The mixed alkali effect, in: A.F. Wright and J. Dupuy (Eds.), Glass...current issues, Martinus Nijhoff, Dordrecht, 1985, p. 456-456.
[102] J.O. Isard, The mixed alkali effect in glass, J. Non-Cryst. Solids 1 (1969) 235-261.
[103] D.E. Day, Mixed alkali glasses - Their properties and uses, J. Non-Cryst. Solids 21 (1976) 343-372.

Figure Captions

Fig. 1 Composition of multicomponent glass samples as measured by EDX. Dotted lines represent the target value.

Fig. 2 Density and molar volume of the multicomponent $40P_2O_5{\cdot}(16\text{-}x)CaO{\cdot}20Na_2O{\cdot}24MgO{\cdot}xSrO$ glasses.

Fig. 3 DSC traces of the multicomponent glass samples, showing T_g, T_c and T_m.

Fig. 4 FTIR spectra for the multicomponent glasses. The dotted lines indicate prominent bands in the spectra, and their positions are given in cm^{-1}.

Fig. 5 Solid state MAS NMR spectra of the multicomponent glasses: (a) ^{31}P, and (b) ^{23}Na.

Fig. 6 Distinct scattering, $i(Q)$, of (a) binary metaphosphate, and (b) multicomponent glasses $40P_2O_5{\cdot}(16\text{-}x)CaO{\cdot}20Na_2O{\cdot}24MgO{\cdot}xSrO$ glass, where x is 0, 4, 8, 12 and 16 mol% SrO.

Fig. 7 Total correlation functions, $T(r)$, of (a) binary glasses, and (b) multicomponent glasses, where the region before the vertical line at 1.8 Å was Fourier transformed using the step modification function, and the region after the dotted line was Fourier transformed using the Lorch modification function [48]. Thick coloured lines are for experimental data, whilst thin black lines indicate fitted peaks (individual components are shown dashed, and sums of components are shown continuous).

Fig. 8 The pH of the dissolution media (ultra-pure water) at each time point for each of the multicomponent glasses.

Fig. 9 The average mass loss per unit area ($g\ cm^{-2}$) for multicomponent glasses in ultra-pure water. The insert shows the dissolution rate ($g/cm^2/hrs$) for each multicomponent glass (n=3) in ultra-pure water, deionised water (DI) and phosphate buffered saline (PBS) – see text for details.

Fig. 10 Cumulative cation release profiles from the multicomponent glasses investigated, which were degraded in ultra-pure water. The inset on each graph shows the ion release rates normalised to the surface area.

Fig. 11 Comparisons between various total correlation functions, $T(r)$, evaluated using only the Lorch modification function [48], unless stated otherwise. a) MgP_2O_6 glass (blue, continuous line) compared with a simulation for crystalline $Mg_2P_4O_{12}$ [80] (black, dashed line). b) Comparison of multicomponent glasses evaluated using the step modification function for distances shorter than 1.8 Å. c) MgP_2O_6 glass (blue, thick line) compared with P40 glass (black, thin line). The inset shows the two correlation functions in the region of the Mg-O peak, after division by the Mg-O coefficient (Eqn. 3) so as to yield the Mg-O partial correlation function, $t_{MgO}(r)$.

Fig. 12 Total correlation functions, $T(r)$, of multicomponent glasses, together with the results obtained by simultaneously fitting all five functions simultaneously using a specially

developed version of the programme NXFit [92]. See text for details of the fitting, and see legend for explanation of the various lines.

Fig. 13 The correlation functions of the multicomponent glasses P40 and Sr16, after subtraction of the P-O, Na-O, Ca-O and Sr-O peaks; see the text for details. Also shown are examples of atomic environments giving rise to shorter and longer Mg-O bonds. The central (red) atom is a NBO, bonded to one phosphorus (small sphere), one Mg atom (intermediate size sphere), and either one or two other modifier cations (e.g. Sr, large spheres).

Fig. 14 The Mg-O (closed symbols) and O…O (open symbols) parameters for peak fits to the correlation functions, $\Delta T(r)$, of the multicomponent Sr-series glasses, after subtraction of the P-O, Na-O, Ca-O and Sr-O peaks; see the text for details of the subtraction. The lines are guides to the eye. a) The RMS variation in distance ($\left\langle u^2_{\mathrm{MgO}} \right\rangle^{½}$ and $\left\langle u^2_{\mathrm{O\ldots O}} \right\rangle^{½}$, a measure of the peak width), b) the coordination number (n_{MgO} and $n_{\mathrm{O\ldots O}}$), and c) the mean interatomic distance (r_{MgO} and $r_{\mathrm{O\ldots O}}$).

Fig. 15 The total atom number density, and the partial atom number densities for oxygen, phosphorus and strontium in the multicomponent glasses.